MARMARA UNIVERSITY
INSTITUTE FOR GRADUATE STUDIES
IN PURE AND APPLIED SCIENCES

FLOW BOILING CORRELATIONS FOR CO_2 USING ANN AND GA METHODS

AHMET KORKMAZ

MASTER THESIS
Department of Mechanical Engineering

Thesis Supervisor
Assoc.Prof.Dr.MEHMED RAFET ÖZDEMİR

Thesis CO- Supervisor
Asst.Prof.Dr.SEMİH ÖZEL

ISTANBUL, 2023

MARMARA UNIVERSITY
INSTITUTE FOR GRADUATE STUDIES
IN PURE AND APPLIED SCIENCES

FLOW BOILING CORRELATIONS FOR CO_2 USING ANN AND GA METHODS

AHMET KORKMAZ

(524620011)

MASTER THESIS
Department of Mechanical Engineering

Thesis Supervisor
Assoc.Prof.Dr.MEHMED RAFET ÖZDEMİR

Thesis CO- Supervisor
Asst.Prof.Dr.SEMİH ÖZEL

ISTANBUL, 2023

MARMARA UNIVERSITY
INSTITUTE FOR GRADUATE STUDIES IN PURE AND APPLIED SCIENCES

Ahmet KORKMAZ, a Master of Science student of Marmara University Institute for Graduate Studies in Pure and Applied Sciences, defended his thesis entitled "Flow Boiling Correlations for CO_2 Using ANN and GA Methods", on February 20, 2023 and has been found to be satisfactory by the jury members.

Jury Members

Assoc. Prof.Dr. Mehmed Rafet ÖZDEMİR (Advisor)
Marmara University .....(SIGN) .....

Assoc.Prof. Özlem ŞENVAR (Jury Member)
Marmara University .....(SIGN) .....

Assist.Prof. M. Alper ÖZPINAR (Jury Member)
Istanbul Commerce University .....(SIGN) .....

APPROVAL

Marmara University Institute for Graduate Studies in Pure and Applied Sciences Executive Committee approves that Ahmet KORKMAZ be granted the degree of Master of Science in Department of Mechanical Engineering, Engineering Faculty on February 20, 2023 (Resolution no: .....).

Director of the Institute
Prof. Dr. Bülent EKİCİ

ACKNOWLEDGMENT

I would like to express appreciation to my advisors Assoc. Prof. Dr. Mehmed Rafet ÖZDEMİR and Asst. Prof. Dr. Semih ÖZEL for their sincere guidance in my academic life.

I am eternally grateful to my beloved wife and children for the endless patience, self-confidence, and endurance they have given me.

I would also like to express my gratitude to the esteemed BAP members for their unwavering support. This work was supported by Marmara University BAP unit under the project code FYL-2022-10426.

February 2023 **Ahmet KORKMAZ**

INDEX

ACKNOWLEDGMENT i

INDEX ii

ÖZET iiv

ABSTRACT vi

SYMBOLS viii

ABBREVIATIONS xi

LIST OF FIGURES xiiii

LIST OF TABLES xiv

1. INTRODUCTION 1

1.1. Two Phase Flow Boiling Patterns in Horizontal Pipes 4

1.2. Objective 8

1.3. Scope 8

2. LITERATURE REVIEW 10

3. CO2 FLOW BOILING HEAT TRANSFER COEFFICIENT WITH CLASSICAL EQUATIONS AND GENERAL INTRODUCTION OF ANN METHOD 20

3.1. CO2 Flow Boiling Heat Transfer Mechanism 20

3.2 An Introduction to Artificial Neural Network 27

3.3 Concepts of Artificial Neural Network 29

3.4. Working Principle of the Artificial Neural Network 30

3.4.1. Back propagation 32

3.4.2. Back propagation with gradient descent 32

3.5. Overfitting and Preventing Methods 34

3.5.1. Simplifying the model 34

3.5.2. Early stopping 34

3.5.3. Using of regularization 35

3.5.4. Using of dropouts 36

4. MATERIALS AND METHODS 37

4.1. Multilayer Perceptron 37

4.2. Introduction of GA 39

4.2.1. Failure of gradient-based methods 40

4.2.2. Genetic algorithms fundamentals 41

5. RESULTS AND DISCUSSIONS 45

5.1. MLP Neural Network Model 1 46

5.2. MLP Neural Network Model 2 47

5.3. Eureqa GA Model 48

5.3.1 Factor Analysis with R Studio 51

5.4. MLP Neural Network Model 3 52

5.5. Discussion 53

6. CONCLUSION 60

REFERENCES 63

APPENDICES 68

CURRICULUM VITAE 73

ÖZET

ANN VE GA YÖNTEMLERİ KULLANILARAK CO_2 KAYNAMALI AKIŞ KORELASYONLARI

Günümüzde fosil yakıtlar, petrol ürünleri ve benzeri sistemler, özellikle soğutucu gazlar, ozon tabakasına ciddi zararlar vermekte ve küresel ısınmaya neden olmaktadır. Özellikle Küresel Isınma Katsayısı (GWP) ve ozon tabakası hasar potansiyel katsayısı (ODP) günümüzün en önemli konuları arasında yer almaya devam etmektedir. Bilim adamları ve öncü devletler çözüm olarak güneş enerjisi, rüzgâr enerjisi ve nükleer enerji gibi yenilenebilir kaynaklara yönelik çalışmalar yapsa da, küresel ısınma ve ozon tabakası riski hala önemli bir problem olarak karşımıza çıkmaktadır.

Genel olarak soğutucu akışkanların bu olumsuz etki üzerinde çarpan etkisi yaratması araştırmacıları farklı alternatif gazları araştırmaya itmiştir. Bu zararlı gazların başında R22, R12, R11, R134A vb. gelir. Bu tür gazlar ozon tabakasına ciddi şekilde zarar verir. Bu nedenle, kullanımları kademeli olarak kısıtlanır veya yasaklanır. Araştırmalar sonucunda, amonyak ve CO_2 gibi geçmişte bilinen ve halen üzerinde çalışılan gazlardan yararlanma fikri ortaya çıkmıştır. CO_2, ucuzdur, doğada bol miktarda bulunur, toksik değildir ve sıvı olarak taşınabilir. Birçok yönden alternatiflerinden daha iyi performans gösterir. En önemlisi GWP değerinin 1 ve ODP değerinin 0 olmasıdır. Konvansiyonel gazlı soğutmalı akışkanlara göre bu oran çok düşüktür.

Diğer avantajlı yönlerinden bir tanesi de kullanım alanı olarak öne çıkmaktadır. Özellikle hassas elektronik cihazların soğutulması gibi uygulamalarda kullanılmaya başlanmıştır. Örneğin, İsviçre'deki CERN projesinde yüksek hassasiyetli soğutma gerektiren cihazlarda CO_2'li soğutma uygulamalarına başlanmıştır. Ayrıca İngiltere'de yaygın olarak kullanılan gaz soğutmalı reaktörlerde de yoğun olarak kullanılmaktadır.

Birçok araştırmacının CO_2 üzerinde yaptığı çalışmaların sonucunda CO_2'nin çift fazlı kaynamalı akış durumunda çekirdekli kaynama (nükleotit) bölgesinde veriminin en yüksek olduğu kanıtlanmıştır. CO_2'nin nükleoit bölgesinde birçok faz ortaya çıkmaktadır. Örneğin, kuru fazlı akış, dairesel fazlı akış, kesikli-dalga fazlı akış, kabarcık fazlı akış vb. birçok faz vardır. Araştırmacılar, CO_2'nin hangi faz aralığında daha verimli çalıştığını anlamak için deneysel ve teorik olarak farklı yöntemler geliştirmiş ve farklı korelasyonlar

ortaya koymuş veya mevcut korelasyonları daha da geliştirerek en yüksek doğrulukta ısı transfer katsayısını veren korelasyonu bulmaya çalışmışlardır. Ancak, 90%'ın üzerinde doğruluk oranına sahip bir çalışma henüz elde edilememiştir. Araştırmacılar, neredeyse benzer test koşulları altında bile meydana gelen mantıksız sapmaların nedenini açıklayamamıştır. Farklı çalışmalarda elde edilen deneysel veriler, farklı ısı transfer katsayıları ortaya çıkarmıştır. Yüksek doğrulukta bir korelasyon ortaya koymak ve bunu klasik matematiksel veya nümerik yöntemlerle ispatlamak çok zordur.

Tez çalışması CO_2 için yeni bir ısı transfer katsayısı korelasyonu ortaya koyma amacı taşımaktadır. Bu çalışmada yapay zekâ kullanılarak 80%'in üzerinde doğrulukla bir ısı transfer katsayı modeli çıkarılmaya çalışılacaktır. Modelde kullanılan veriler daha önce laboratuvar ortamlarında elde edilmiş deneysel veriler olacaktır. Modelde, nükleotid bölgesinde ortaya çıkan tüm fazları kapsayan ortak bir korelasyon geliştirilecektir. Bu korelasyon genel olarak tüm fazları kapsayacağından, her aşama için ayrı ayrı oluşturulmaya çalışılan mevcut korelasyonlara alternatif olarak araştırmacılara kolaylık sağlayacaktır.

Çok katmanlı algılama yöntemi (MLP), Genetik algoritma (GA) ve faktör analizi sırayla kullanılacaktır.

Böylelikle, mevcut klasik korelasyonlara alternatif bir korelasyon ortaya çıkarılmış olacaktır.

ABSTRACT

FLOW BOILING CORRELATIONS FOR CO_2 USING ANN AND GA METHODS

Today, fossil fuels, petroleum products, and similar systems, especially refrigerant gases, cause severe damage to the ozone layer and cause global warming. Especially the Global Warming Coefficient (GWP) and ozone layer damage potential coefficient (ODP) continue to be among today's most critical issues. Although scientists and pioneering states work on renewable resources such as solar, wind, and nuclear energy as a solution, the risk of global warming and the ozone layer is still a significant problem.

In general, the fact that refrigerants have a multiplier effect on this adverse effect has pushed researchers to investigate different alternative gases. Some of these harmful gases are R22, R12, R11, R134A, etc. Such gases seriously damage the ozone layer. Therefore, their use is gradually restricted or banned. As a result of the research, the idea of utilizing gases such as ammonia and CO_2, known in the past and still being studied, emerged. CO_2 is inexpensive, abundant in nature, non-toxic and, transportable. In many ways, it outperforms its alternatives. The most important is that the GWP value is unity, and the ODP value is 0. This ratio is very low compared to conventional gas-cooled fluids.

One of its other advantageous aspects is its usage area. It has started to be used in applications such as cooling-sensitive electronic devices. For example, in the CERN project in Switzerland, CO_2 cooling applications have been started in devices that require high-precision cooling. It is also used extensively in gas-cooled reactors, which are widely used in the UK.

As a result of the studies carried out by many researchers on CO_2, it has been proven that the efficiency of CO_2 is highest in the nucleate boiling region in the case of two-phase boiling flow. Many phases emerge in the nucleate boiling region of CO_2. For example, dry phase flow, annular phase flow, pulsed-wave phase flow, bubbly phase flow, etc. There are many phases. Researchers have developed different experimental and theoretical methods to understand which phase range CO_2 works more efficiently. They have revealed different correlations or tried to find the correlation that gives the highest

accuracy heat transfer coefficient by further improving the existing correlations. However, a study with an accuracy rate above 90% has yet to be obtained. Experimental data obtained in different studies revealed different heat transfer coefficients. The researchers could not explain why the unreasonable deviations occurred even under similar test conditions. Establishing a highly accurate correlation and proving it using classical mathematical or numerical methods is almost impossible.

The thesis study aims at developing a new heat transfer coefficient correlation for CO_2. In this study, a heat transfer coefficient model is worked out, which yields an accuracy of over 80%. The data used in the model will be experimental data previously obtained in laboratory environments. A common correlation in the model is developed, covering all phases in the nucleate boiling region. Since this correlation will cover all stages in general, it will provide convenience to researchers as an alternative to existing correlations that are tried to be created separately for each stage.

Multi-layered detection method (MLP), Genetic Algorithm (GA), and factor analysis are going to be used in order.

Thus, an alternative correlation will be proposed and substituted with the existing correlations.

SYMBOLS

A : Pipe cross section area, [m^2]

A_{LD} : Liquid section diameter, [m^2]

A_{VD} : Vapor section diameter, [m^2]

a : Learning rate, [-]

b : Bias, [-]

Bo : Bond number, [-]

c_{pl} : Liquid specific heat capacity, [KJ/kgK]

c_{pv} : Vapor specific heat capacity, [KJ/kgK]

D : Pipe diameter, [m]

D_{eq} : Equivalent diameter, [m]

F : Transfer function, [-]

Fr_l : Froud number liquid, [-]

g : Gravitational accelaration [m/s^2]

G : Mass flux, [kg/m^2s]

G_M : Mist flow mass flux, [kg/m^2s]

h_{tp} : Total heat transfer coefficient, [kW/m^2K]

h_v : Dittus Boelter heat transfer coefficient, [kW/m^2K]

h_{cb} : Convective boiling heat transfer coefficient, [kW/m^2K]

h_{nb} : Nucleate boiling heat transfer coefficent, [kW/m^2K]

h_{wet} :Wet perimeter heat transfer coefficient, [kW/m^2K]

k_l : Liquid thermal conductivity, [kW/mK]

k_v : Vapor thermal conductivity, [kW/mK]

L1 : L1 regularization, [-]

L2 : L2 regularization, [-]

P_r : Reduced pressure, [Pa]

P_{crit} : Critical pressure, [Pa]

P_{total} : Total pressure, [Pa]

Pr_l : Liquid Prandtl number, [-]

Pr_v : Vapor Prandtl number, [-]

R : Regression model, [-]

R^2 : R^2 squared regression model (goodness of fit), [-]

Re_l : Liquid Reynold number, [-]

Re_v : Vapor Reynold number, [-]

Re_δ : Liquid film Reynolds number

S : Nucleate boiling suppression factor, [-]

T_{sat} : Saturation temperature, [K]

Q : Heat flux, [kW/m^2]

$Q_{crit.}$: Critical Heat flux, [kW/m^2]

w_i : Weight value, [-]

w_x : New weight, [-]

We_l : Liquid Weber number, [-]

We_v : Vapor Weber number, [-]

x : Vapor quality, [-]

x_{di} : Vapor quality during transition from dry zone to intermittent zone, [-]

x_{ia} : Transition vapor quality during transition from intermittent flow to annular, [-]

X_{tt} : Martinelli number, [-]

y_k : Output value in splitted time k, [s]

Greek Symbols

α **:** White noise error, [-]

δ **:** Thickness of annular liquid film, [m]

ϵ **:** Void fraction, [-]

ϕ **:** Activation function, [-]

μ_l **:** Liquid viscosity, [kg/ms]

μ_v **:** Vapor viscosity, [kg/ms]

θ **:** Dry angle, [radian]

ρ_l : Liquid density, [kg/m^3]

ρ_v **:** vapor density, [kg/m^3]

σ **:** Surface tension, [kg/m^3]

ABBREVIATIONS

AI : Artificial intelligence

ANN : Artificial Neural Network

AR : Automatic Regression

EXP : Experimental

GA : Genetic Algorithm

GWP : Global Warming Potential

IA : From Intermittent to annular flow

MA : Moving Average

MAPE : Mean absolute Percentage Error

MLP : Multi-layer Perceptron

MSE : Mean Square Error

ODP : Ozone Depletion Potential

PRED : Predictive

SAT : Saturation

SQP : Sequential Quadratic Programming

LIST OF FIGURES

Figure 1.1. Thermodynamic property diagram of CO_2, Cavallini et al. (2022).

Figure 1.2. Two phase boiling flow regimes, Hrnjak et al. (2007).

Figure 1.3. Flow regime map of Kattan et al. (1998a).

Figure 2.1. Surface tension vs. evaporation temperatures, Bansal and Zhao (2010).

Figure 2.2. The density ratio of liquid to vapor evaporation temperature, Bansal and Zhao (2010).

Figure 2.3. The experimental boiling heat transfer data at low saturation temperature at -10°, Bredesen et al.(1997).

Figure 2.4. The experimental boiling heat transfer data at low saturation temperature at -25°, Bredesen et al.(1997).

Figure 2.5.a Comparison of CO_2 with other cooling gases at T=10°C, G=400kg/m^{2}s saturation temperature, Hrnjak et al. (2011).

Figure 2.5.b Comparison of CO_2 with other cooling gases at T=10°C, G=200kg/m^{2}s saturation temperature, Hrnjak et al. (2011).

Figure 3.1. Experimental test setup, Oh et al. (2011).

Figure 3.2. Forming of flow patterns, Oh et al. (2011).

Figure 3.3. Schematic diagram of film thickness, Kandlikar (2002).

Figure 3.4 (a). Figure 3.4 (b) Yun et al. (2005) CO_2 two phase flow pattern.

Figure 3.5. Schematic sketch of biological and artificial neuron design, Takafumi et al.(2007).

Figure 3.6. Schematic sketch of single layer perceptron, Phil (2017).

Figure 3.7. Schematic sketch multi layer perceptron, Allam (2019).

Figure 3.8. Principle of the artificial neural network, Keerthana (2021).

Figure 3.9. Schematic sketch of the back propagation with gradient descent, Adhikari (2019).

Figure 3.10. Schematic sketch difference between big and small learning rate,

Adhikari (2019).

Figure 3.11. Schematic sketch early stopping explanation, Sagar (2019).

Figure 3.12. Schematic sketch of dropouts method before and after applying to the sample model, Sagar (2019).

Figure 4.1. Schematic sketch **s**ingle layer perceptron**,** Phil (2017).

Figure 4.2. Activation function samples, Dosch (2021).

Figure 4.3. Schematic sketch of MLP, Peixoto (2020).

Figure 4.4. Schematic sketch GA working principle, Michalewicz (1990).

Figure 4.5. Figure of failure gradient-based methods**,** Michalewicz (1990).

Figure 4.6. GA elements, Michalewicz (1990).

Figure 4.7. Schematic sketch GA elements, Michalewicz (1990).

Figure 4.8. The basic structure of GA, Michalewicz (1990).

Figure 5.1. Architechture of Model1.

Figure 5.2. Architecture of Model2.

Figure 5.3. Best solutions of different complexities.

Figure 5.4. Solution fit plot.

Figure 5.5. Architecture of Model3.

Figure 5.6. Heat transfer coefficient comparison for D = 6 mm, G = 98-405 kg/m^{2}s. T_{sat} = 243-273K, x=0.04-0.82, Q = 4.9-15.50 kW/m^2

Figure 5.7. Heat transfer coefficient comparison for D = 7 mm, G = 200 kg/m^2 s, T_{sat} = 248-263K, x=0.14-0.95, Q = 6 kW/m^2.

Figure 5.8. Heat transfer coefficient comparison for D =10 mm, G = 80 kg/m^2 s, T_{sat} = 245K, x=0.15-0.82, Q = 8 kW/m^2.

Figure 5.9. Heat transfer coefficient comparison for D =11.20 mm, G = 40-200 kg/m^2 s, T_{sat} = 243-258K, x=0.09-0.82, Q = 5-10 kW/m^2

LIST OF TABLES

Table 1.1. Comparison of different refrigerants in terms of GWP and ODP, Tiejun et al. (2013)

Table 2.1. Literature studies on the CO_2 heat transfer coefficient

Table 3.1. Flow pattern transition equations, Cheng (2008).

Table 3.2. Comparison of L1 and L2, Sagar (2019).

Table 5.1. General factors of models

Table 5.2. Results of MLP Model1.

Table 5.3. Results of MLP Model 2.

Table 5.4. Results of the Eureqa GA model.

Table 5.5. Variable Sensitivity Results.

Table 5.6. R studio factor analysis results

Table 5.7. Results of MLP model 3

Table 5.8. Comparison of mean square error between applied methods.

Table 5.9. Analysis of the heat transfer coefficients for our expected flow boiling.

Table 5.10. Several empirical correlations for the estimation of CO_2 boiling heat transfer (before dry-out)

Table 5.11. Mean deviation absolute error for 4.35mm diameter pipe.

1. INTRODUCTION

Although CO_2 has been a known gas for many years, it has been used in limited areas for certain reasons. CO_2 is cheap, abundant in nature, easily storable, liquid transportable and non-toxic, which outperforms its alternatives in many ways, Dennis et al. (2014). The most important thing is that the GWP value is one, and the ODP value is shown in Table 1.1. This ratio is very low compared to conventional gas-cooled fluids. Besides being a naturally produced gas, low GWP and ODP values increase its widespread usage.

Table 1.1. Comparison of different refrigerants in terms of GWP and ODP, Tiejun et al. (2013)

Refrigerant	GWP	ODP	Atmospheric Life (years)
R11	3.800	1	50
R12	8.100	1	102
R134a	1.300	0	13.60
R717-Ammonia	0	0	-
R744-CO_2	1	0	-
R290-Propne	3	0	-

CO_2 started to be used especially as a refrigerant gas in the 1990s, Maina et al. (2015). There were some issues in the use of carbon dioxide because of operating at high critical pressures and low critical temperature. However, CO_2 has started to be used in devices such as mobile air conditioners, compressors, residential heat pumps, hot water heat pumps, which are already suitable for working at 4MPA by the means of the developing technologies. Due to this outstanding feature, it has even started to be used in atomic power plants. As a given example, it has even started to be used in nuclear cogeneration systems, Qil, et al. (2018). It is assumed that it will recover all the waste heat energy by using flow boiling heat transfer as liquid carbon dioxide at 20°C instead of water.

Meanwhile, CO_2 has different thermophysical properties contrary to conventional gases as well. Figure 1.1 shows the thermodynamic properties of CO_2. CO_2 is a gas with very variable properties at different pressures and saturation temperatures compared to other gases. (see Appendix B-Table B.1)

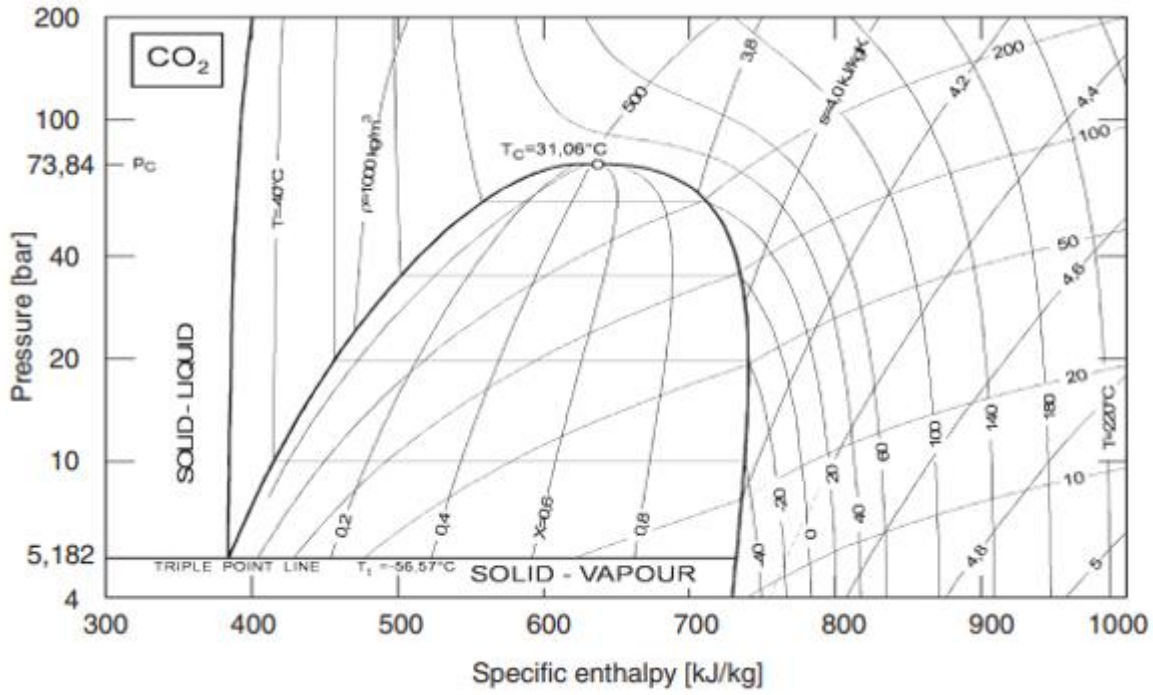

Figure 1.1. Thermodynamic property diagram of CO_2, Cavallini et al. (2022).

Cheng, L. et al. (2006) found that none of the heat transfer coefficient correlations for CO_2 in boiling flow and two phase flow did not highly confirm the obtained results in experimental studies. They have shown that this is actually due to the missing factors in the correlations with their research. Although many correlations have been defined in later studies, it has become almost impossible to verify correlations with experimental data as validation in studies such as Cheng et al. (2008), Thome et al. (2004), and Yagov (2009). Even though scientists proposed correlations in single-phase flows in horizontal pipes to simplify the phenomenon, they could not fully elucidate the process due to the difficulty of momentum and energy transfer in two phase flow. Nevertheless, the proposed estimation method has been accepted as a general method just for single-phase flows and adding some empirical values to be simplified the process. In most cases that cover the total heat transfer coefficient equation in nucleate boiling, additional empirical factors were used to overlap the flow boiling results with the experimental data. However, more physically accurate correlations need to be created. Consequently, it is clear enough that the main reason for deviations from experimental data on two-phase flow and heat transfer is not the specific properties of one substance or the other but the lack of a true theory of the process. As shown in Figure 1.2, there are many patterns in flow boiling process. The researchers tried to form separate correlations for each region or a general

correlation covering a few of them in their studies. However, a general correlation that can cover all patterns could not be established due to the reasons mentioned above mathematical model is so complex that it is almost impossible to create; accordingly, not much success can be achieved numerically. For this reason, scientists have tried to form a better correlation by changing or adding some factors to existing valid correlations to complement each other. Even with some restrictions, they could only work in a certain range of diameters, heat flux, vapor quality, and mass flux. Meanwhile, the scarcity of experimental data continues to hinder the studies carried out noticed by Yagov (2019), Cheng et al. (2008).

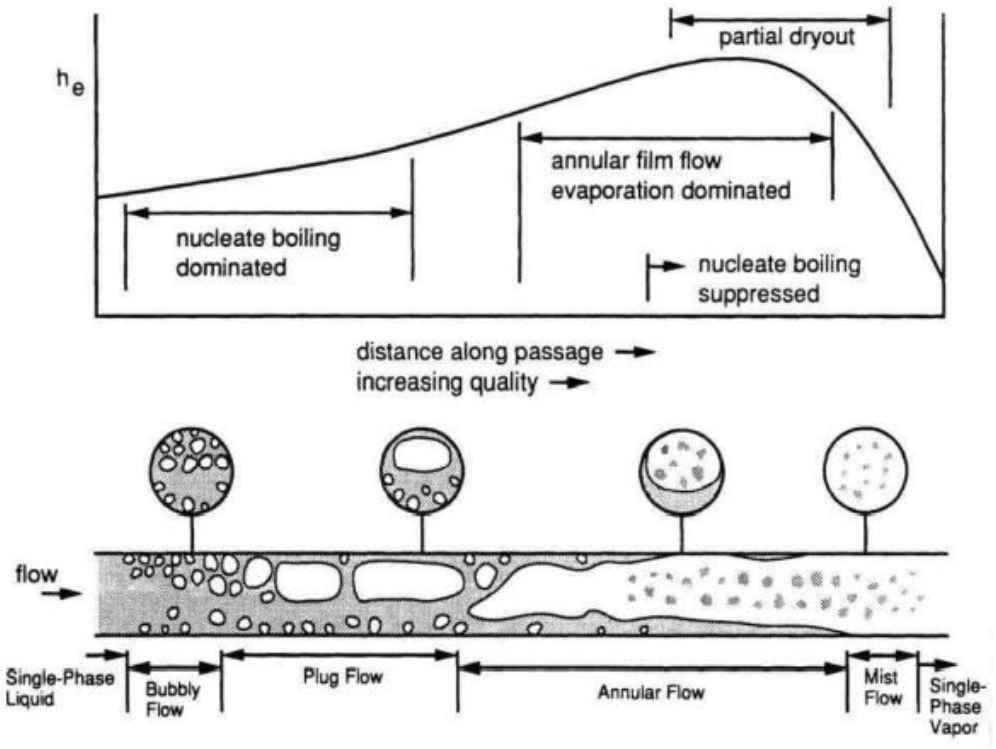

Figure 1.2. Two phase boiling flow regimes, Hrnjak et al. (2007).

Although CO_2 yields the best heat transfer coefficient in the nucleate boiling region and also enhances the researchers to work on these patterns, unfortunately, a high-accurate correlation could not be established for the patterns in all phases noticed by Cheng et al. (2008), Gungor et al. (1987). The use of missing factors in the correlations has made this even more complex and unknown. Due to the essential impossibility of forming a substantial mathematical description of flow boiling heat transfer, there are also different methods of obtaining the prediction equations for heat transfer coefficient, such as

numerical methods, and artificial intelligence.

The proposed model with the artificial intelligence method is considered to provide a precise equation covering all patterns and also provide an analysis of the patterns to understand the main process precisely. It is determined the effects of each data on the correlation in terms of process optimization. It is to be done by optimizing by considering the weights of each data in the equation in the regression process. After optimization, it is to be generated new correlation, which is an alternative to existing correlations. As a result, more detailed information below about flow patterns is presented to be envisaged in the case.

1.1. Two Phase Flow Boiling Patterns in Horizontal Pipes

It has presented the different flow pattern zones that describe the flow patterns superficially based on Thome, J. R. (2015). It can be classified patterns as bubbly flow, stratified flow, stratified wavy flow, plug flow, slug flow, annular flow, intermittent flow, and mist flow.

Table 1.2. The Flow Patterns in Horizantal Pipes, Thome J.R.(2015).

Figures	Explanation
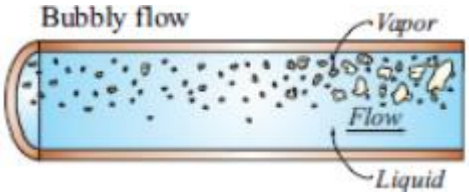 **Figure 1.3.** Bubbly flow	Bubbly flow in the liquid phase has many gas bubbles. The bubbles are denser on the pipe's upper wall due to the liquid's buoyancy. They generally show uniform distribution because of shear forces in the liquid.

Table 1.2. The Flow Patterns in Horizantal Pipes, Thome J.R.(2015). (**continued**)

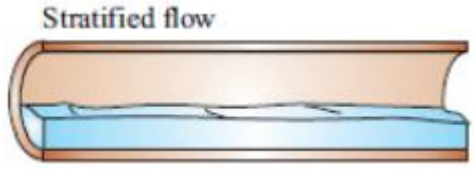 **Figure 1.4.** Stratified flow	Stratified flow's buoyancy forces are more effective at low liquid and gas velocities. The separation of two phases is executed during gas moving along the upper part of the channel and the liquid along the lower part of the tube. It is almost flat, with no significant waves between the two phases. Mainly, half of the pipe is dry; the rest is wet.
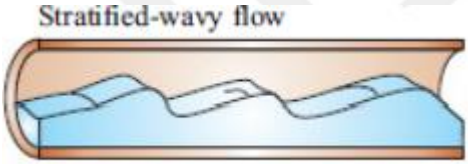 **Figure 1.5.** Stratified-wavy flow	Stratified-wavy flow forms once the gas velocity exceeds the liquid velocity, and waves form on the liquid due to shear forces. However, the upper part of the pipe remains mostly dry.
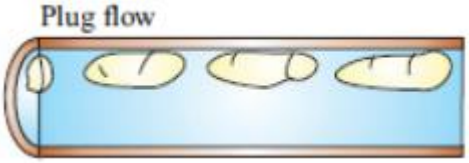 **Figure 1.6.** Plug flow	Large, extended gas bubbles in a liquid flow characterize the plug flow regime. It originates from the channel's upper section. The liquid phase is continuous because the extended bubbles' diameters are less than the tube's.
 **Figure 1.7.** Slug flow	Slug flow is observed once the gas flow increases. Elongated gases commence resembling slug flow obtained in vertical flow channels through the tube.

Table 1.2. The Flow Patterns in Horizantal Pipes, Thome J.R.(2015). (**continued**)

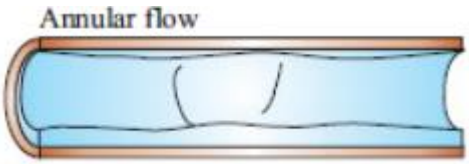 **Figure 1.8.** Annular flow	Annular flow forms once the liquid is forced into annular flow due to the raising of gas velocity like at vertical flow. The liquid thickness gets thicker on the lower wall and slightly thinner on the upper wall. If the gas velocity continues to increase, a dry area will form at the top surface of the pipe.
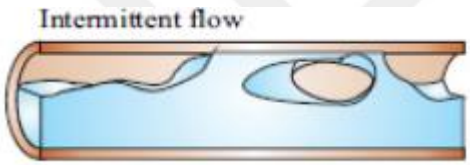 **Figure 1.9.** Intermittent flow	Intermittent flow forms once gas velocity is further increased to wet the top of the pipe. Thus, enough film layer is formed to almost wet the upper side of the pipe.
 **Figure 1.10.** Mist flow	Mist flow is the transition of the liquid film into gas form, being further thinner. This process proceeds in droplet form, which starts at the top of the pipe surface. Thus, an entrainment form of small droplets occurs in the gas phase.

Researchers set correlations by creating flow pattern maps according to the specifications between mass flow and vapor quality, including all of the flow patterns described above. Researchers tried to determine the heat transfer coefficient by establishing certain connections on the flow pattern map showing the phase transitions. Many researchers include some additional coefficients and logarithmic additions to get a better result. The researchers could not look at the event as a whole and tried to produce local solutions with appropriate coefficients in the transition phases. Another disadvantage of the studies

is that all could be made with restricted experimental inputs, which are already known, such as mass flow and heat flow. The sample flow regime map constructed by Kattan et al. (1998a) can be seen in Figure 1.3.

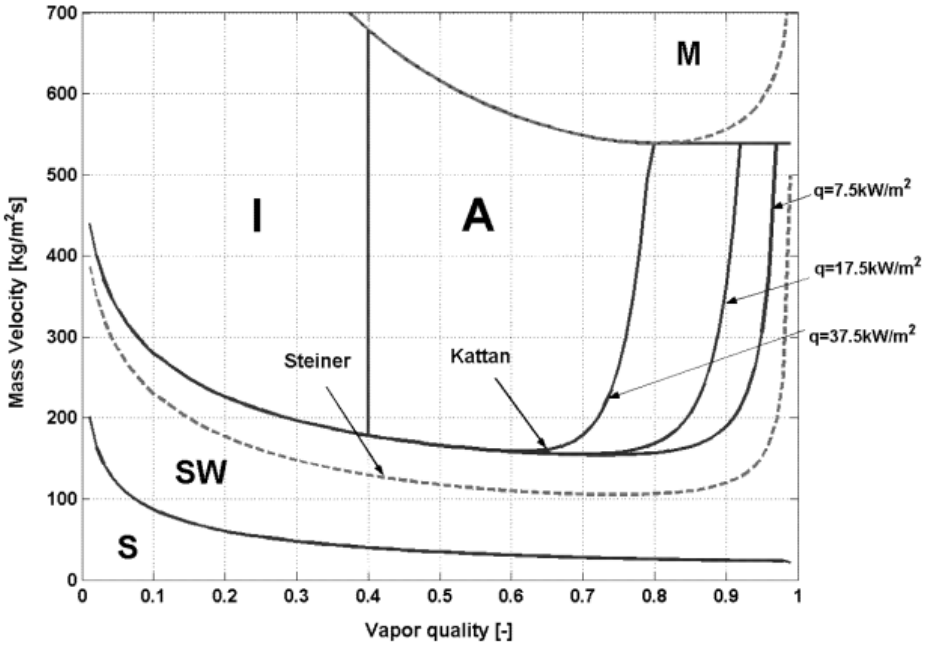

Figure 1.3. Flow regime map of Kattan et al. (1998a).

As shown in Figure 1.3, the flow pattern map is divided into regions where the vapor quality is ranged between zero and one. Vapor quality is defined as the ratio of the amount of vapor to the amount of liquid in a pipe section. The S region represents the slug flow, the SW region represents the wavy slug flow, the I region represents the intermittent flow, the region A represents the annular flow region, and finally, the M region represents the mist flow.

This study proposes a mathematical model with a common solution covering all the phases using an artificial neural network. This is developed using different neural network methods, such as ML and GA methods. Twenty-six different inputs, one output, and 1017 experimental data are used in the model (please see Appendix C). This study aims to help further investigations on CO_2, which can be easily obtained and harmless to nature, will be more eligible to be used, and the versatility of usage areas become so extended. By paving the way for researchers, it aims to develop solutions without dealing with the non-linear ways of carbon dioxide in two-phase flow boiling applications.

1.2. Objective

This study aims to develop a mathematical model using an artificial neural network for carbon dioxide using about 1017 distinctive experimental data performed in the past (see Appendix C). The proposed assessment model focuses on providing heat transfer coefficient estimation or protection for different flow patterns of carbon dioxide. Also, the model developed in this study can be effectively adapted to the other gases which behave nonlinearly as CO_2. It may also be used to help for increasing of CO_2 heat transfer coefficient industrial productivity and performance in the long and medium term and monitor the sustainability of productivity by providing meaningful feedback. On the other hand, the model in question can be transformed into a systematic structure, which can significantly facilitate the analysis of applications and can be developed with sufficient experimental data.

Based on these objectives, three distinctive MLP model is formed and tested with Colab Tensor Flow Notebook. Additionally, the GA method is implemented for optimization, and R studio is used for factor analysis. In conclusion, data segregation was made to mitigate the undesirable results and produce a new correlation in place of existing ones.

1.3. Scope

Since the proposed model here is intended to evaluate the flow-boiling heat transfer coefficients for CO_2, a general model covering all pattern has been developed. However, the model will be validated by manually running on a certain number of experimental inputs from different sources such as Hrnjak, P.S.et al. (2007).

In the thesis, the first section consists of general usage areas of CO_2 and emphasizes its superior properties and disadvantages to other gases. Section two reviews the literature of the studies conducted on the heat transfer coefficient assessments for CO_2 in terms of classical correlations and current neural network studies. Section two mainly focuses on articles about measuring and assessing heat transfer coefficient correlations in literature. The third section includes a general introduction to the CO_2 heat transfer coefficient mechanism and presents an overall review of ANN. Part four will be a general introduction to the AI and also GA methods used for the precise solution. In section five,

Will be generated a couple of models by testing our experimental data on these methods as identified in part four. Afterwards, result and discussings will be assessed and evaluated based on literature studies. In section six, it will be discussed to comment on the new correlation and present a comprehensive assessment from various aspects.

2. LITERATURE REVIEW

Existing studies were used to establish the technical infrastructure of the study. In particular, studies made with classical ANN methods and GA were compiled and interpreted in the conclusion section. Unfortunately, there is no study on the CO_2 heat transfer coefficient using GA. There are only a few optimization studies to increase waste heat energy efficiency in power plants, such as nuclear or solar energy plants, presented by Thanganadar et al. (2019) and Liangxing et al. (2022).

To that end, the following passages are explained briefly to provide the prevailing literature studies regarding the CO_2 heat transfer coefficient.

In their study, Lunda and Aursanb (2014) proposed two different two-phase flow models for CO_2. This model is demonstrated by the statistical rate approach evaluating of evaporation and condensation properties of CO_2. They have benefited from the backward Euler method while solving mathematical functions such as hyperbolic conservation law and ordinary differential equations. A model similar to phase change was issued by examining CO_2 thermodynamic properties and cooling facilities that show the phase change phenomenon of CO_2. This model was compared and combined with a similar pattern representing a two-phase flow. Thus, the heat transfer coefficients were tried to be established by simulation the pressure loss in a pipe using the statistical rate theory. However, it seems essential to validate the model and test it experimentally for more common and valid usage in the future.

In their 2016 study of CO_2, Mikielewicz and Jakubowska provided the model's predictions for the heat transfer coefficient of CO_2 during flow boiling. Experimental data from numerous investigations were combined. Calculations were made for all variations and a wide range of mass velocities. The study's primary purpose is to test the model's accuracy. The results showed the importance of reduced pressure and surface tension in the wall. For this purpose, the correlations of Müller-Steinhagen and Heck (1986) and Friedel (1979) were used. The experimental results showed consistency with obtained results very well. Based on the analyses in the comparisons, deviations are observed in the high vapor quality range. It is observed that the deviations reach almost 59.50%. After thoroughly studying the model, an empirical correction was added to the reduced pressure. As a result, the reduced pressure did not directly affect the heat transfer coefficient but kept the result

stable.

Bansal and Zhao (2010) examined the heat transfer coefficient of CO_2 at degrees in their article. They compared the most recent correlation results with existing correlations. It has been determined that CO_2 has very different properties at low temperatures than other gases. However, they emphasized that more studies should be done due to the need for more experimental data. Therefore, they tried to figure out how the thermal physical properties of CO_2 affect the transfer coefficient at saturation temperatures. The result obtained according to the saturation temperatures are schematized in Fig.2.1 and Fig.2.2 below.

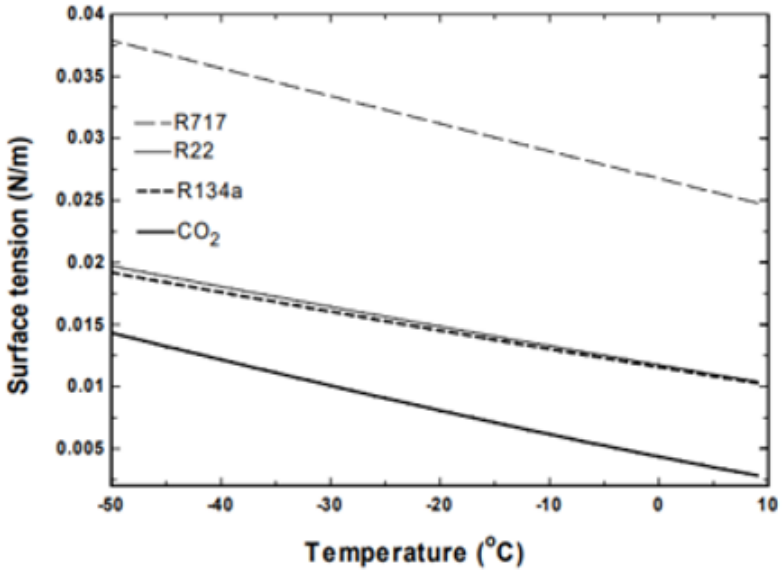

Figure 2.1. Surface tension vs. evaporation temperatures, Bansal and Zhao (2010).

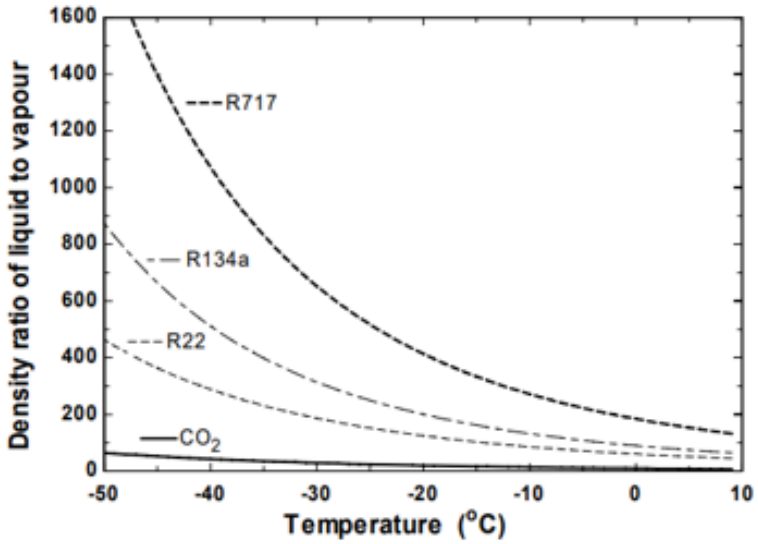

Figure 2.2. The density ratio of liquid to vapor evaporation temperature, Bansal and Zhao (2010).

The conclusion to be drawn from this study is the following. CO_2 has a high density in vapor qualities lower than 0.2 degrees at. The Reynolds number is low in two-phase flow. The flow is mainly in the form of stratified and stratified wavy flow. However, the boiling heat transfer coefficient is lower than at high temperatures. The two-phase flow Reynolds number is higher if vapor quality exceeds 0.2. Due to the high Reynolds number, the flow is more unsteady and circular. The convective heat transfer increased up to the dry phase due to the thin film thickness layer and the liquid's high vapor quality. The nucleate boiling heat transfer decreases due to the more significant surface tension at low saturation temperatures; on the contrary, the convective boiling heat transfer is strengthened because of the higher density ratio of liquid to vapor and thermal conductivity. The experimental boiling heat transfer data at low saturation temperatures of -10°C, -25°C, and -28°C are compared with the currently available empirical correlations in Figure 2.3. and Figure 2.4.

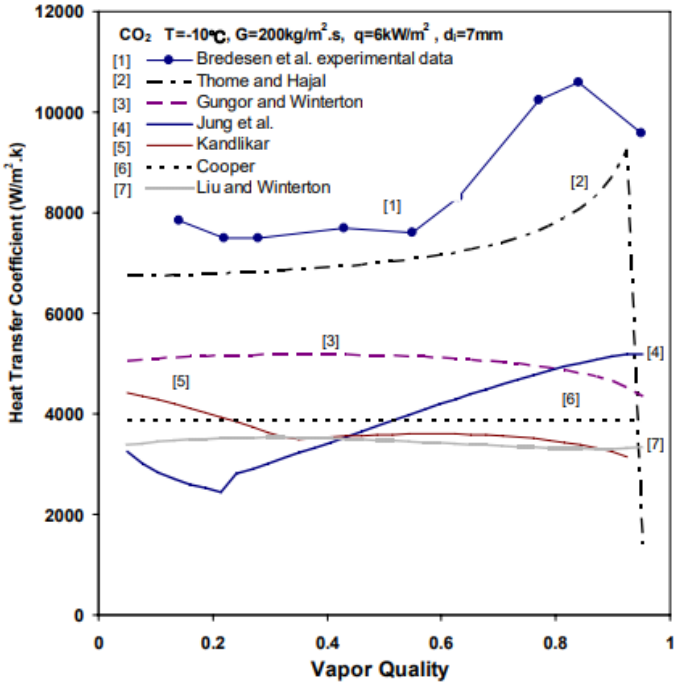

Figure 2.3. The experimental boiling heat transfer data at low saturation temperature at -10°C, Bredesen et al.(1997).

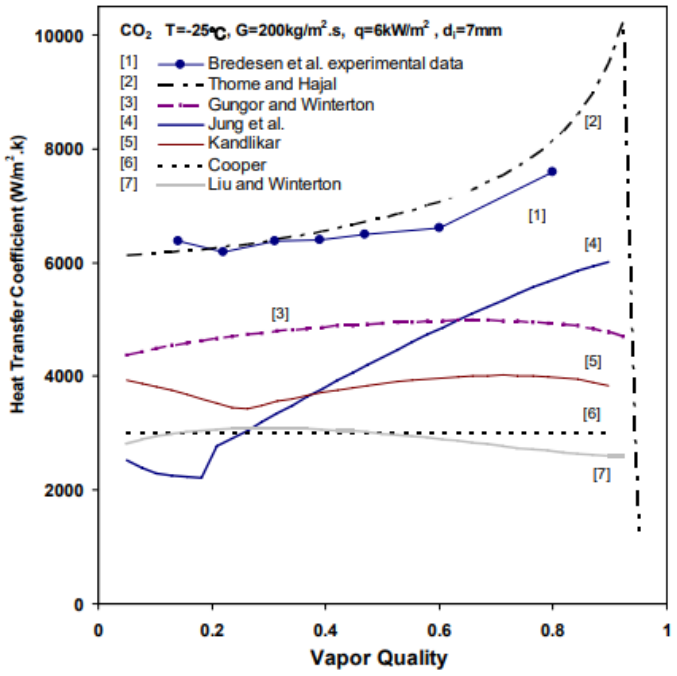

Figure 2.4. The experimental boiling heat transfer data at low saturation temperature at -25°C, Bredesen et al.(1997).

Most correlations present a similar trend with the experimental data but with more significant mean deviations. There is a need for more experimental research and the

development of new empirical boiling heat transfer correlations for CO_2 at low temperatures.

Cheng et al. (2006) developed a new boiling flow model for CO_2 in horizontal pipes in their study. In their first study, they investigated the effects of low pressure and heat flux on the flow boiling heat transfer coefficient at low vapor qualities. Another positive research is namely issued as a new suppression factor in nucleate boiling flow. While creating this correlation, factors such as liquid film thickness and pipe diameters were integrated and correlated. Lastly, a correlation was developed for the starting point of the dry region zone. In the new model map, a correlation was formed based on the heat transfer coefficient for the transition from intermittent flow to annular flow and also from annular flow to dry flow. The accuracy rate of the model is 75.5%. A variety of conditions can be used with the flow boiling heat transfer model and the flow pattern map. Application ranges from 0.8 to 10 mm for tube diameters (equivalent diameters for non-annular channels), 170 to 570 kg/m^2 s for mass velocities, 5 to 32 kW/m^2 for heat fluxes, and 28 to 25 °C for saturation temperatures (reduced pressures from 0.21 to 0.87).

The projected outcomes are mostly tenable and encouraging in light of the wide range of experimental data from various laboratories, particularly some experimental data indicating negative heat transfer tendencies. The drying zone heat transfer estimation is less accurate than other flow regimes due to the deficiency of complete dry-out data. Future improvements are possible if some experimental data becomes available.

Cheng et al. (2008) updated the previous study issued in 2006 under the part I article. A general flow pattern flow boiling heat transfer model was developed for CO_2. The updated flow boiling model applies to a broader range of conditions compared to the first study. It is applicable to tube diameters from 0.6 to 10 mm, mass velocities from 50 to 1500 kg/m2 s, heat fluxes from 1.8 to 46 kW/m2, and saturation temperatures from -28 to 25 °C (reduced pressures from 0.21 to 0.87). In addition, a heat transfer correlation for mist flow was newly proposed, and heat transfer in the bubbly flow regime was added to the model. The updated model was compared with an extensive experimental database of 1108 data points covering 790 new data points. Desired results between the predicted and experimental data were monitored.

Hrnjak et al. (2011) investigated the two-phase flow boiling heat transfer coefficients of

different gases in horizontal pipes in their study. The gases used in the study are R-22, R134-A, R-410A, C3H8, and CO_2. The test ranges were arranged as 50-600kg/m2s mass flux and 5-40KWm2 heat flux. The saturation temperatures were taken at 0-10 degrees. The pipe diameters used in the test equipment were 0.5, 1.5, and 3mm diameters and made of stainless steel. The main purpose of the experiment is to investigate the effects of mass flux, saturation temperature, pipe diameter, and heat flux on the heat transfer coefficient. As a result, the experimentally obtained heat transfer coefficients were compared with some existing correlations, and accuracy was found with a deviation of 15.28%.

Figure 2.5.a and Figure 2.5.b shows the difference between the heat transfer coefficients of R22, R-134a, R-410A, C3H8 and CO_2 under some experimental conditions. High nucleate boiling of CO_2 under the same test conditions made the heat transfer coefficient higher than other gases. In addition, CO_2 has a lower surface tension value under the same conditions. The fact that CO_2 has a lower μ_f / μ_g viscosity ratio under the same conditions causes forming a thin wall on the pipe. This means that the resulting film layer can be stretch and damaged more easily. In addition, the fact that the ρ_f / ρ_g density ratio of CO_2 is lower under the same conditions causes nucleate boiling to be dominant and also lead to low vapor flow.

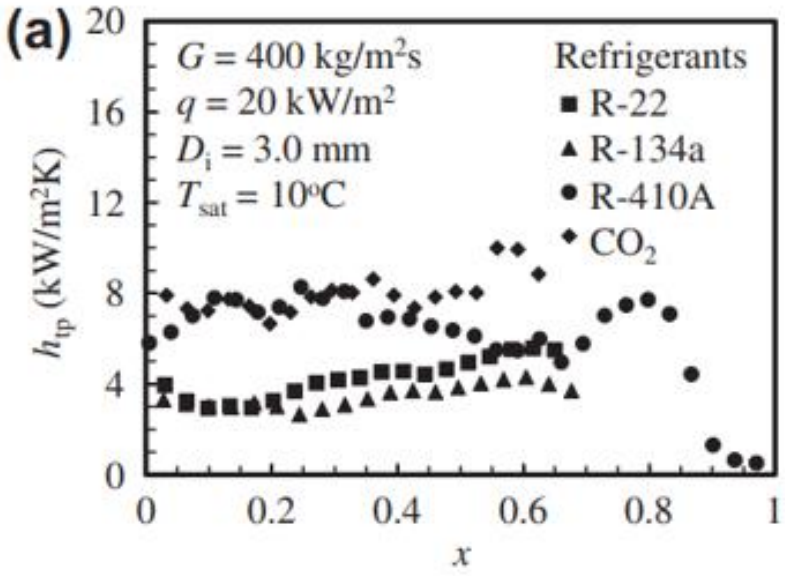

Figure 2.5.a Comparison of CO_2 with other cooling gases at T=10°C, G=400kg/m^{2}s saturation temperature, Hrnjak et al. (2011).

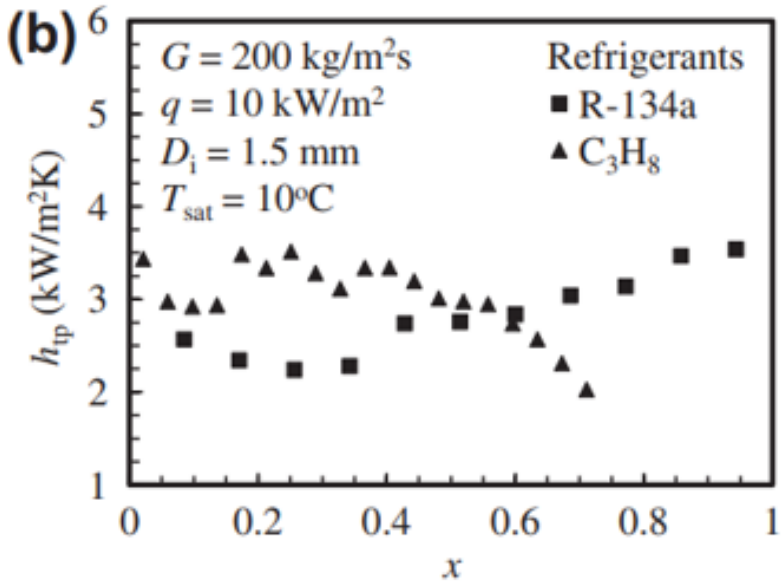

Figure 2.5.b Comparison of CO_2 with other cooling gases at T=10°C, G=200kg/m^{2}s saturation temperature, Hrnjak et al. (2011).

Below is an example of the only artificial intelligence study in the literature on CO_2 by Feng et al. (2021). This study is similar to the thesis topic.

Feng et al. (2021) worked on neural networks for supercritical CO_2 flow. They presented this study as a leading trigger force that will contribute to energy systems. The difficulty of solving nonlinear correlations with classical methods pushed them to use artificial neural networks. They used MATLAB as the program. Thermomechanical property values were investigated by assigning three different patterns. They used 5895 data in total. They found mean square error (MSE) smaller than 3.11%. This is proof of the superiority of ANN to classical correlations. These studies can play a leading role in designing more efficient energy systems in the future.

Thanganadar et al. (2019) have worked on the idea of utilizing the waste heat in power plants by taking advantage of the high critical temperatures of CO_2 with the Brayton cycle. In cases in which the CO_2 turbine temperature input is 550 degrees and above, it is more efficient and more stable than other classical Rankine and Joule-Brayton cycles. Since the problem is not linear, they used the SQP program (Sequential Quadratic Programming) to get a highly accurate result. Since the SQP program was scanty to reach an optimum result, they incorporated the GA Non-Dominated Sorting GA heuristic method into SQP to make a hybrid study. Eventually, it achieved 48.32% efficiency at

600°C and 50.25% efficiency over 650°C.

Liangxing et al. (2022) studied on heat exchanger optimization which was performed in the reactor where liquid lead and supercritical CO_2 were used at the coolant side and heating side respectively. Objective function adoption was performed with a non-dominated sorting GA II method based on entropy generation number and pump power. As a result, 25% more efficiency was achieved in the heat transfer coefficient.

In the literature studies, the following observations were determined for two phase flow boiling of CO_2.

(1) As a result of the extensive literature review, some evaluations were made for CO_2. Due to its thermophysical properties, CO_2 showed different properties compared to other conventional gases between 0-25°C temperatures. Compared to other low-pressure refrigerants like R134a and ammonia, etc., CO_2 has significantly higher evaporation heat transfer and far smaller two-phase frictional pressure drops. CO_2 drying occurs at lower vapor qualities because of the predominance of nucleate boiling, contrary to conventional gases which drying occurs at higher vapor qualities. Thereby, nucleate boiling is dominant at high saturation temperatures and low vapor qualities. Compared to other gases, the saturation temperature is more effective on the heat transfer coefficient.

(2) It is very peculiar to obtain different heat transfer coefficient values under equivalent test conditions. It is very difficult to explain this situation thermophysical. The reason can be insufficient precise sensitivity of the measuring devices or incomplete or inaccurate measurement factors. For these reasons, more precise measurements should be made using sensitive test equipment and tools.

(3) Cheng et al. (2006) have obtained extremely successful solutions in other flow patterns, such as intermitted, intermitted wavy, slug flow, etc., rather than mist flow and dry flow models. However, more studies and tests are required to establish a valid correlation in dry and mist flow pattern regions.

(4) CO_2 has been researched for use in a variety of practical applications, including the cooling of electronic chips, the development of an evaporative CO_2 cooling system for the CMS pixel detector, and the potential for the production of renewable energy and electricity. Therefore, efforts should be made to examine unknown CO_2 evaporation applications in the applicable sectors.

As observed in the literature studies shown in Table 2.1, it is difficult to have a fully valid correlation for two-phase flow boiling for CO_2. Therefore, either using different methods or tools that provide high-accuracy solutions is needed, Hrnjak et al. (2011) study shows that the artificial neural network method could be used in creating new correlations for investigating the heat transfer coefficient of CO_2. AI will provide flexibility to create a new correlation for each pattern and phase in high rate accuracy, which covers all phases in discrepancy.

Another technical issue was the difficulty of optimizing the model owing to the complexity of the CO_2 heat transfer coefficient thermophysical properties. In this case, the researchers tried to reach the solution by using the heuristic GA approach methods. Likewise, in the thesis study, a model is to be tried to be produced using the classical MLP method. Afterward, the segregation of inputs from outliers and a new correlation will be issued.

Table 2.1. Literature studies on the CO_2 heat transfer coefficient

Data Source	Study	Method
Liangxing et al. (2022)	Studies for Lead-to-Supercritical Carbon Dioxide Heat Exchanger Based on Genetic Algorithm	GA method
Thanganadar et al. (2019)	Off-Design and Annual Performance Analysis of Supercritical Carbon Dioxide Cycle	GA and ANN methods
Feng et al. (2021)	Thermomechanical properties of CO_2 in critical region	Artificial Intelligence

The difference between this study from the studies in Table 2.1 is that both MLP and GA methods were used and revealed a correlation with higher accuracy. In addition, a more comprehensive range of results will be obtained versus those previously obtained only with specific and limited temperature, mass flow, diameter, and steam quality values.

3. CO2 FLOW BOILING HEAT TRANSFER COEFFICIENT WITH CLASSICAL EQUATIONS AND GENERAL INTRODUCTION OF ANN METHOD

3.1. CO2 Flow Boiling Heat Transfer Mechanism

The energy attenuation rate in the modern world is rising daily. Energy efficiency is tried to be ensured in every field, and research is enforced to design systems as efficiently as possible. In particular, it is aimed that the gases used in cooling systems should impact less damage to the environment as well as materialize the efficiency. CO_2 is one of these gases, and CO_2 provides the best efficiency in the nucleate flow boiling region since it has a high reduced pressure and a low critical temperature compared to other gases. Therefore, the flow boiling heat transfer coefficient of CO_2 in the evaporation temperatures ranging from -25 to 0 shows different characteristics contrary to other conventional gases, such as R134a, studied by Bansal and Zhao (2010). The fact that it depends on many different factors makes it impossible to carry out a mathematical or numerical model while establishing correlations. None of the presented correlations yields an active applicable mechanism directed to measuring and evaluating the results at a substantial accuracy rate.

For each fluid, a specific mechanism system should be created to assess the heat transfer coefficient. Figure 3.1 demonstrates how to calculate the CO_2 heat transfer coefficient to examine the patterns formed in the laboratory unit investigated by Oh et al. (2011). The test equipment components are explained in the following respectively. The test can be applied to the pipe, either keeping the constant heating or holding at a constant temperature. As can be seen from Figure 3.2, the CO_2 is compressed by the pump and reaches high pressure, then passes through the heater, and the phase patterns in the pipe are observed. Then, it reaches the condenser for cooling down. From here, it is transferred to the main tank, and the process is repeated as a closed loop. The lengths of the pipes generally range from 1m to 3m depending on the test setup.

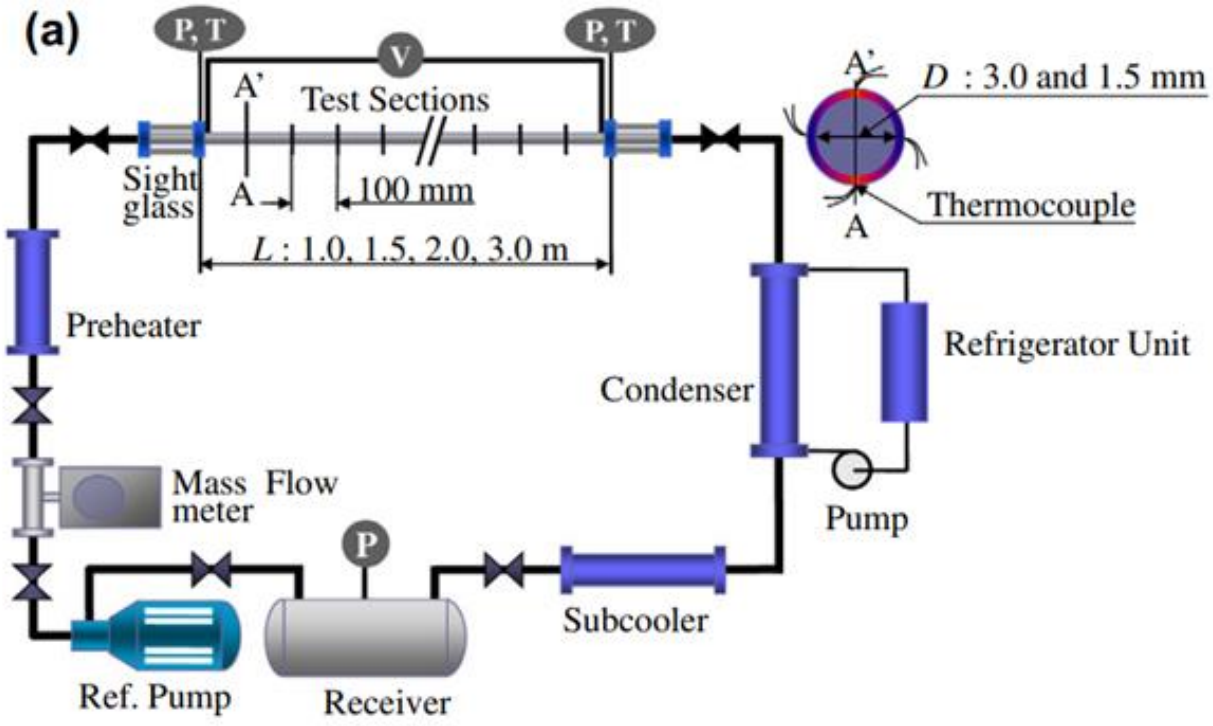

Figure 3.1. Experimental test setup, Oh et al. (2011).

It can be seen two phase flow boiling patterns easily in Figure 3.2 in the study, Oh et al. (2011).

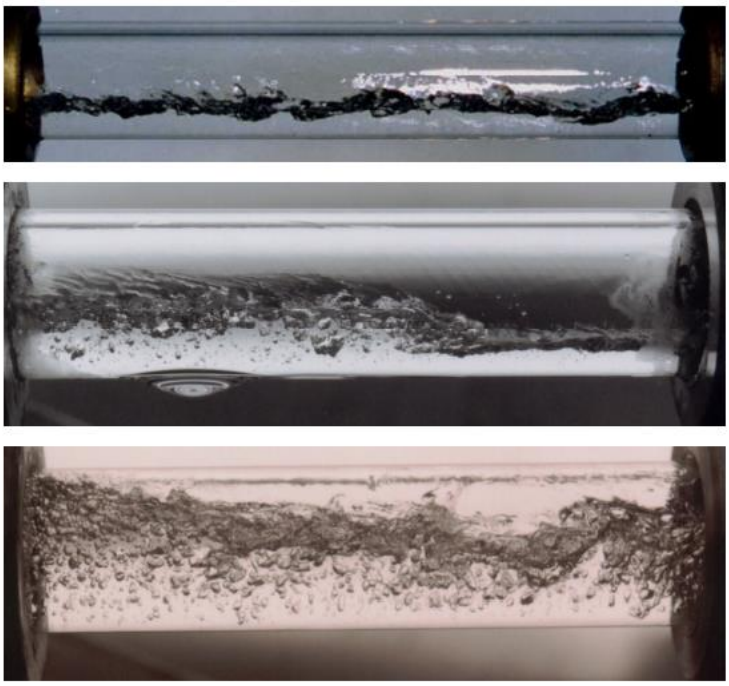

Figure 3.2. Forming of flow patterns, Oh et al. (2011).

In order to understand the heat transfer coefficient of CO_2, it should be explained very well of macro and microchannel terms, see Appendix A-TableA.1. Expressed by Kandlikar (2002), hydraulic diameter ranges ($D_{h)}$ are expressed as follows, referring to different classifications:

- Conventional channels: $D_h > 3$ mm.
- Minichannels: $D_h = 200$ μm – 3 mm.
- Microchannels: Dh =10 μm – 200 μm

Another issue is the structure of flow patterns. These need to be understood within two criteria: first, the appraising of heat transfer in evaporative heat transfer, and the other one is the complexity of the two-phase flow phenomenon. In this case, a flow pattern map should be settled, and this map is needed to predict the local flow pattern in a channel. When the literature is checked, it is seen that many flow model maps have been developed to determine the two-phase flow patterns occurring in horizontal pipes. Many of these flow maps were developed for adiabatic conditions irrespective of diabatic conditions. In this case, big differences/contradictions have emerged.

Because of its physical characteristics, CO_2 has strong nucleate boiling heat transfer properties in intermittent flows with low vapor quality. As a result, scientists created several diabatic flow patterns associated with the heat transfer coefficient. However, none of these apply to CO_2 evaporation in horizontal pipes because CO_2 has very low surface tension and high reduced pressures, which significantly impact its two-phase flow properties. A sudden drop in heat transfer coefficients will identify phase transitions. The general equations that researchers have developed thus far in this area are as follows:

The abrupt decrease of the heat transfer coefficients between the two flow regimes indicates the distinction between the intermittent and annular flow. At the same time, an abrupt decrease in heat transfer indicates the onset of drying. The distinction between dry zone and annular flow is determined in this case.

According to the experimental studies, the following Intermittent–Annular and Annular–Dry transition factors are solved for CO_2, with a correlation by Cheng (2008).

Table 3.1. Flow pattern transition equations, Cheng (2008).

Pattern Explanation	**Equation**
Intermittent–Annular and Annular–Dry transition correlation	$x_{IA} = \left[1.8^{1/0.875} \left(\frac{\rho_v}{\rho_l} \right)^{-1/1.75} \left(\frac{\mu_v}{\mu_l} \right)^{-1/7} + 1 \right]^{-1}$
Transition boundary of the drying zone	$G_{dryout} = \left\{ \frac{1}{0.236} \left[\ln\left(\frac{0.58}{x} \right) + 0.52 \right] \left(\frac{D_{eq}}{\rho_v \sigma} \right)^{-0.17} \left[\frac{1}{g D_{eq} \rho_v \left(\rho_l - \rho_v \right)} \right]^{-0.17} \left(\frac{\rho_v}{\rho_l} \right)^{-0.25} \left(\frac{Q}{Q_{crit}} \right)^{-0.27} \right\}^{1.471}$
Dry-inginitial equation	$x_{di} = 0.58 e^{\left[0.52 - 0.236 We_V^{0.17} Fr_V^{0.17} \left(\frac{\rho_v}{\rho_l} \right)^{0.25} \left(\frac{Q}{Q_{crit}} \right)^{0.27} \right]}$

Table 3.1. (continued) Flow pattern transition equations, Cheng (2008).

Transition boundary from the drying zone to the mist flow

$$G_M = \left\{ \frac{1}{0.502}\left[\ln\left(\frac{0.61}{x}\right) + 0.57 \right]\left(\frac{D_{eq}}{\rho_V \sigma}\right)^{-0.16}\left[\frac{1}{gD_{eq}\rho_V\left(\rho_V - \rho_l\right)}\right]^{-0.15}\left(\frac{\rho_V}{\rho_l}\right)^{0.09}\left(\frac{Q}{Q_{crit}}\right)^{-0.72} \right\}^{1.613}$$

G_M for the case where the entire wall is dry:

$$x_{de} = 0.61e^{\left[0.57 - 0.502 We_V^{0.16} Fr_V^{0.15}\left(\frac{\rho_V}{\rho_l}\right)^{-0.09}\left(\frac{Q}{Q_{crit}}\right)^{0.72}\right]}$$

The transition boundary from intermittent to bubbly flow

$$G_B = \left\{ \frac{256 A_{VD} A_{LD}^{\ 2} D_{eq}^{\ 1.25} \rho_l \left(\rho_l - \rho_v\right) g}{0.3164\left(1 - x\right)^{1.75} \pi^2 p_r \mu_l^{\ 0.25}} \right\}^{1/1.75}$$

It is very important that a general heat transfer coefficient correlation method provides the precise outputs obtained from the experimental data. In this case, the two-phase flow must be expressed physically in relation to heat transfer mechanisms, flow pattern transitions, and corresponding flow patterns. Changes in the flow pattern map also have an impact on the heat transfer correlation. Therefore, these data are applied separately to flow patterns to find a common correlation that covers all the phases. A general evaporative heat transfer model has been developed for a wider range of conditions and covers all flow regimes by Kattan et al. (1998). Local flow boiling heat transfer coefficients h_{tp} in horizontal pipes is shown in Equation 3.1;

$$h_{tp} = \frac{\theta_{dry} h_v + \left(2\pi - \theta_{dry}\right) h_{wet}}{2\pi} \tag{3.1}$$

The ratio of pipe circumference and flow structures in contact with liquid and vapor is defined as θ_{dry} in equation 3.1. Where θ_{dry} is the dry angle and is shown in Figure 3.3. In stratified flow, the stratified angle θ_{strat} and θ_{dry} are equal. On the other hand, for intermittent (I), annular (A), and bubbling (B) flows, the θ_{dry} value is equal to zero. For stratified-wavy flow, θ_{dry} ranges from zero to its maximum value θ_{strat}. The laminar-wavy flow was divided into three zones to determine θ_{dry}. These are a layered-wavy slug, slug/stratified-wavy, and stratified-wavy.

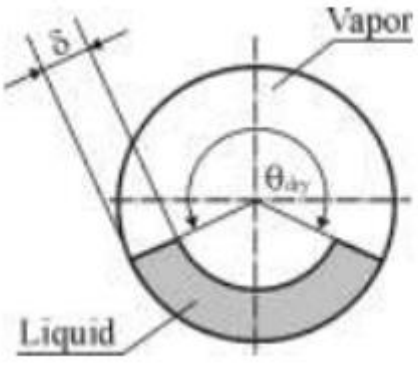

Figure 3.3. Schematic diagram of film thickness, Kandlikar (2002).

Considering the pipe's annular flow with the Dittus and Boelter (1930) correlation, the h_v over the dry environment is calculated. h_{wet} is calculated with an asymptotic model which

combines the contributions of h_{cb} and h_{nb} heat transfers to flow boiling heat transfer by the third power shown in Equation 3.2.

$$h_{wet} = \left[\left(Sh_{nb} \right)^3 + h_{cb}{}^3 \right]^{1/3} \tag{3.2}$$

In the research by Cheng et al., S is assigned to decrease the contribution of nucleate boiling heat transfer caused by the thickness of the annular liquid film (2006).
Where, the annular liquid film thickness is shown in Equation 3.3.

$$\left.\begin{array}{l} \text{If } x_{IA} > x, S = 1 \\ \text{If } x_{IA} < x, S = 1\text{-}1.14 \left(\dfrac{D_{eq}}{0.00753} \right)^2 \left(1\text{-}\dfrac{\delta}{\delta_{IA}} \right)^{2.2} \end{array}\right\} \tag{3.3}$$

Where, h_{nb} is shown in Equation 3.4.

$$h_{nb} = 131 p_r{}^{-0.0063} \left(-\log_{10} p_r \right)^{-0.55} M^{-0.5} Q^{0.58} \tag{3.4}$$

Additionally, utilizing the original model's annular liquid film flow, h_{cb} is calculated as follows by Cheng et al. (2006) and Kattan et al. (1998) in Equation 3.5. Where Re is Reynold Number and k_l is liquid thermal conductivity.

$$h_{cb} = 0.0133 Re_{\delta}{}^{0.69} Pr_l{}^{0.4} \frac{k_l}{\delta} \tag{3.5}$$

As seen from all the equation above, no substantial correlation has been proposed to provide high accurate heat transfer coefficient. Many researchers tried to get more accurate results by improving the existing correlations from each other. In addition, determining correlations put forward high deviations, especially in the mist and dry flow regions. For instance, Yun et al. (2005) compared the estimated flow-boiling heat transfer coefficients with the experimental data and presented them in Figure 3.4 (a). Figure 3.4(b) with the corresponding flow map. As shown below, predicting heat transfer data in mist and drying flow regimes can be challenging. Therefore, any other possible alternative solutions like ANN are sought, which can accurately predict the experimental data in

these identified phases.

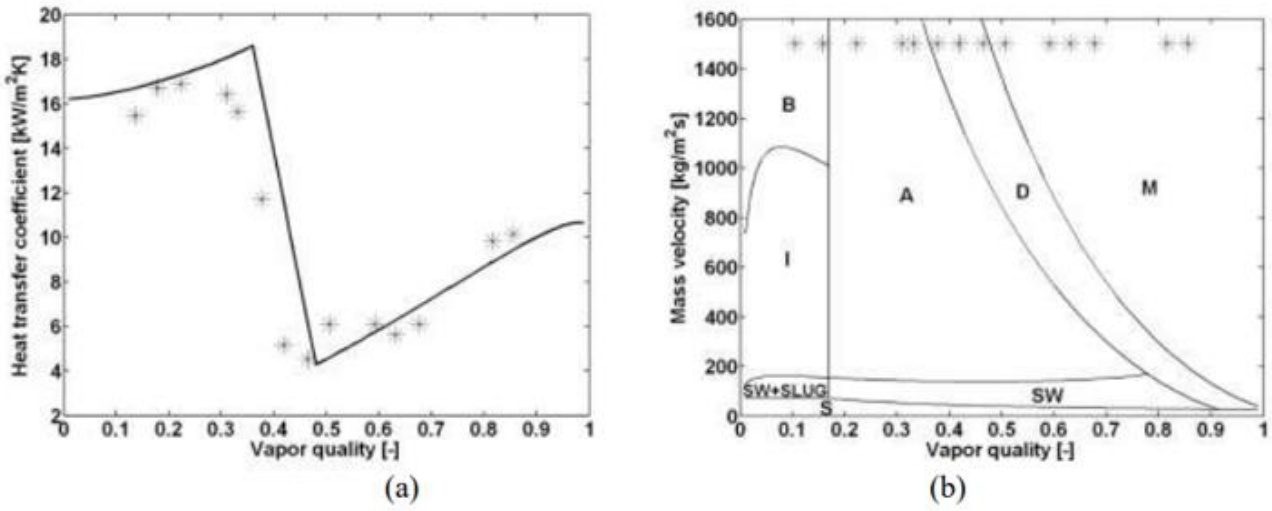

Figure 3.4 (a,b). Yun et al. (2005) CO_2 two phase flow pattern

3.2 An Introduction to Artificial Neural Network

Neural networks are the subject of machine learning used for artificial intelligence. Some nonlinear problems are too difficult to solve and out of the scope of classical algorithms. As a result, it should be beneficial to how widely ANN is used in the contemporary world for that kind of aim. It is used in many fields such as aviation, automotive, chemistry, astronomy, space industry, genetics, qualified fraud detection, radar systems, regression analysis, classification, pattern recognition, decision making, face recognition systems, and classification.

As stated in the study of Guimei et al. (2008), the neural network stands out in such scenarios and can solve very complex problems. ANN can be perceived as the response of the neural networks in the body according to the received responses from the external environment, Osval et al. (2022). Neural networks are connected by layers similar to the neural networks in the human brain. Like traditional machine algorithms, it reacts to logic by training in neural networks. In short, a model has generated both trainings the factor and adding weights with a static bias to the neurons. Afterward, the model is transmitted to different activation functions. After obtaining output from the final neural layer, the loss function which is the error between the expected and calculated results. The weights are adjusted again to find the optimum values for the lost function and create a wise model

to minimize the losses. This model consists of multiplication, addition, and activation. Here, each input is multiplied by a specific weight. It calculates a result by collecting the data whose weights and biases are defined in the sum function in the middle section. ANN at the output evaluates the calculated result, whose weight and bias are defined previously.

Although the working principles of ANN may seem very simple, the main trick is associating these models with ANN. Figure 3.5 describes the artificial and biological neural networks.

ANN uses these basic simple rules when solving complexity. The optimization and topology in the following steps do not mean that the neural network can be used immediately, but it shows that a provision has been met. Before using the model created in ANN, it is necessary to determine the problem mainly. Of course, the most crucial factor here is the size of the experimental data and good segregation, just as in biological neural networks. Biological neural networks have settled on three essential piles: supervised and unsupervised learning and reinforcement learning, Takafumi et al. (2007). The problem is chosen together with these learning paradigms simultaneously. Although the working principles of learning paradigms differ, they all have a common point. The first is learning data, and the other is learning rules. Based on these two basic paradigms, an output is obtained using primary neural networks. After the model of the ANN is determined, optimization is made. Based on this, neural network can now be used to solve the problem correctly.

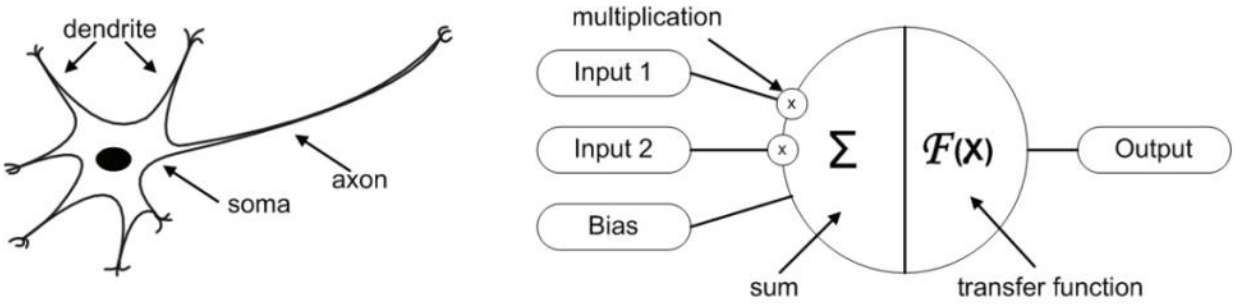

Figure 3.5. Schematic sketch of biological and artificial neuron design, Takafumi et al.(2007).

The data from the external environment comes to the dendrites in the brain. The processed information in the somas is transmitted to the axons. ANN operates precisely on this

paradigm. The given data is processed by taking into account the weights and biases in the neurons to generate a proper output. While doing this, it uses the internal transfer function. The mathematical representation is shown in Equation 3.6., Ben and Patrick (1996).

$$y_k = F\left(\sum_{i=0}^{m} w_i(k) \times x_i(k) + b\right) \tag{3.6}$$

Where $x_i(k)$ is input value for layer-k processing element value, $w_i(k)$ is the weight value for layer-k processing element value, b is bias, F is a transfer function, and $y_i(k)$ is output value for layer-k processing element value

3.3 Concepts of Artificial Neural Network

Input Layer: Obtained inputs from the outside world and also known as the input, is submitted to the model to learn from the main source. Input nodes transmit the data to the next layer, named the hidden layer, Phil (2017).

Hidden Layer: Hidden layers are separate layers in which calculations are made. Their number varies according to the complexity of the problem. A single layer can be used for simpler operations. The number of neurons in it is also chosen to be the most optimal, Phil (2017).

Output layer: Output layers are obtained as multiple or single depending on the type of problem. The obtained results are derived from mathematical derivations in the neural network. More than one result can be observed depending on the type of model to be created. However, the thesis subject will be modeled to obtain a single output, Phil (2017).

Perceptron and multi-layer perceptron: Perceptron is an earliest form of Neural Network and consists of only one layer in which all the calculations are executed, as shown in Figure 3.6.

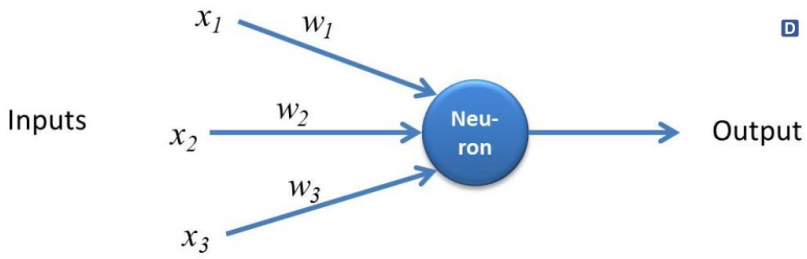

Figure 3.6. Schematic sketch of single layer perceptron, Phil (2017).

Multilayer Perceptron is also an Artificial Neural Networks which consists of multiple perceptions layers together to establish a multilayer neural network shown in Figure 2.7.

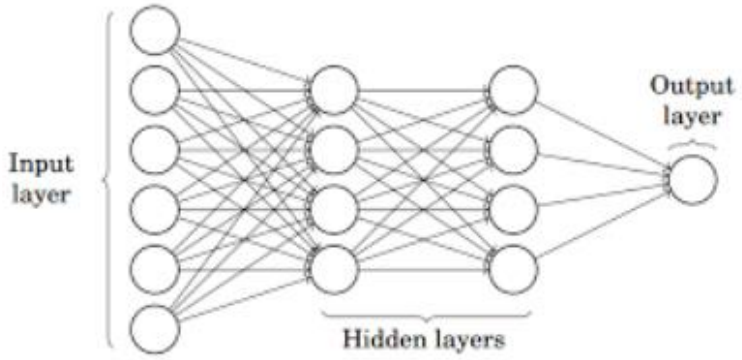

Figure 3.7. Schematic sketch multi-layer perceptron, Allam (2019).

Figure 3.7 can be summarized as follows:

- An input layer, with 6 input nodes
- Hidden Layer 1, with 4 hidden nodes/4 perceptrons
- Hidden layer 2, with 4 hidden nodes
- Output layer with 1 output node

3.4. Working Principle of the Artificial Neural Network

The collected data is transmitted to the hidden layers, respectively. At this stage, weights are updated, and biases are added. The process direction of the data is shown in Figure 3.8 as $x_1, x_2, x_3 \ldots x_n$. Each layer consists of neurons that join with each other. All incoming inputs are subjected to mathematical calculations in the section indicated in the blue circle.

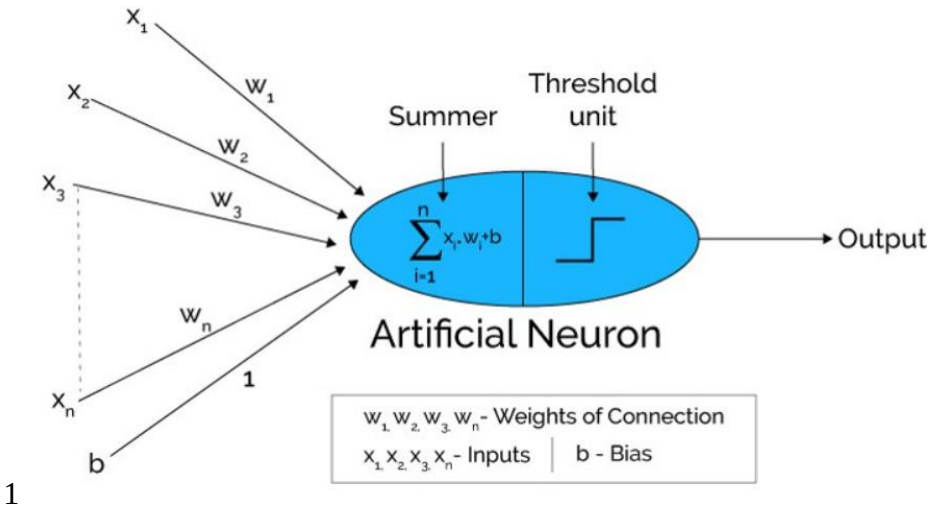

Figure 3.8. Principle of the artificial neural network, Keerthana (2021).

The two steps involved in estimation in hidden layers are as follows:

1. Each input is multiplied by a weight randomly or by known calculations. The weight indicates the equivalent power of each input on the result. After the weights are selected properly, a solution is produced by adding biases. Bias is chosen to give the most optimal solution. This process is simply calculated by open-ended in GA, which will be explained in the optimization issue later on.

2. The generated equation is sent to the activation function in the next step. It is important that the problem is not linear here because ANN is mostly used in complex non-linear problems.

3. The process that carries out in the second item proceeds estimations in a chain manner. The information processed in all hidden layers is transferred to the other layer. This process continues until it reaches the last layer, and an output is obtained as a result.

4. After obtaining the final result, backpropagation is used to make an amendment to the model. This cycle is repeated until the error between the final and the target result is optimum and minimum. Error rates will be used in the thesis based on the mean square error term. Let's explain back propagation below.

3.4.1. Back propagation

Backpropagation helps to underestimate the error difference between the target and the specified values. It tries to do this by optimizing the weights and coefficients. Weights are made using optimization tools. Optimization tools are mathematical equations that change weights to minimize errors in neural networks, Kan (2017).

3.4.2. Back propagation with gradient descent

Gradient descent is one of the optimization tools that help in renewing weights. In the picture below, J_{min} is the curve created to reach the minimum shown in Figure 3.9.

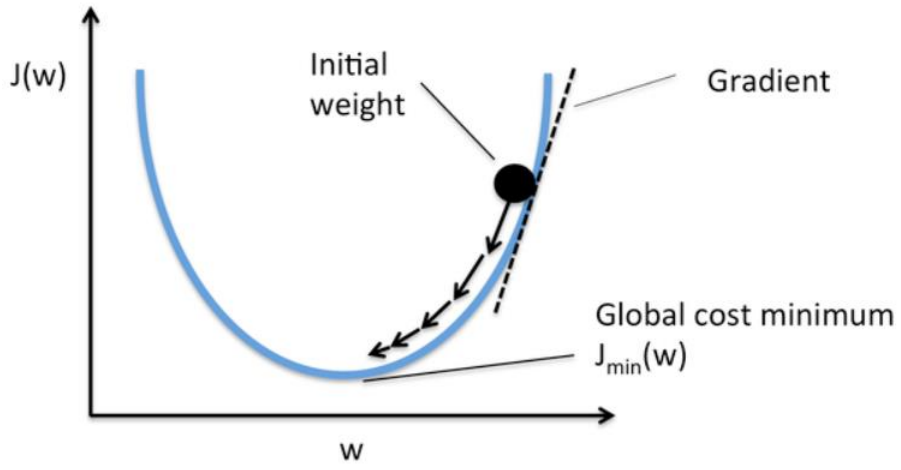

Figure 3.9. Schematic sketch of the back propagation with gradient descent, Adhikari (2019).

These steps should be followed to achieve the global cost minimum:

1. Weights are assigned randomly and the process is started. Results are obtained by performing forward propagation. Mean squared errors are calculated.

2. Then the gradient is the estimated derivative of the error with respect to current weights.

3. Then new weights are calculated using the below equation, where a is the learning rate which is the factor also known as step size to control the speed or steps of the backpropagation. It gives additional control on how fast we want to move on the curve to reach global minima. Ben and Patrick (1996) explain this equation in equation 3.7.

$$
\left.
\begin{aligned}
&W_x = W_x - a\left(\frac{\partial_{error}}{\partial W_x}\right) \\
&W_x : \text{New weight} \\
&a : \text{ Learning rate} \\
&\frac{\partial_{error}}{\partial W_x} : \text{ Derivative of error with respect to weight}
\end{aligned}
\right\} \qquad (3.7)
$$

4. Once the global minimum is attained and the loss is minimized, the process of computing the new weights, calculating the errors in the new weights, and updating the weights is recapped.

The first factor that should be selected in accordance with the model is the learning rate. The learning rate is the change or size of the steps needed to reach the global minimum. Here, it is crucial to keep in mind that the learning rate should be carefully defined in our weight-raising equation. It should not be too big, as this would prevent it from ever reaching global minimums, as illustrated in Figure 3.10, nor should it be too small, as this would delay convergence.

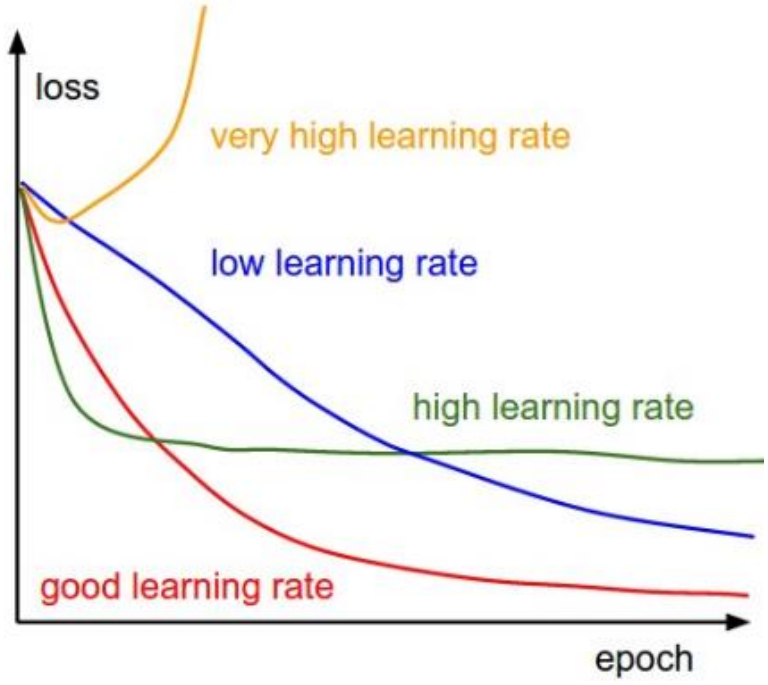

Figure 3.10. Schematic sketch difference between big and small learning rate, Zulkifli (2019).

3.5. Overfitting and Preventing Methods

Overfitting can be reveal out during solving too much noisy problem due to problem has many factors. If the trained model yields better results by using with existing data but gives bad results with untested data in this regard, this model should be inspected. Because the model works by generalizing the existing available data. This is very important as our model yield results with the new data collected in the future.

3.5.1. Simplifying the model

One of the ways to get rid of overfitting is to reduce the complexity of the model. By doing so, we can reduce our neural layers or randomly change the number of neurons. Of course, the input and output values of the layers had to be made sensitively. What size our network should be or how small it should depend entirely on experience.

3.5.2. Early stopping

Early stopping is a regularization problem. An iterative model such as gradient descent can be used when training a model. Since all neural networks use the gradient descent method, this process can be terminated at the optimal point. The model makes recurrent itself with each iteration to reach the best fitting. Proceeding the iteration beyond the point at which the model performs best results in an overestimated generalization and causes an error rate. Early stopping helps prevent this and helps determine how many iterations can be done before overfitting starts.

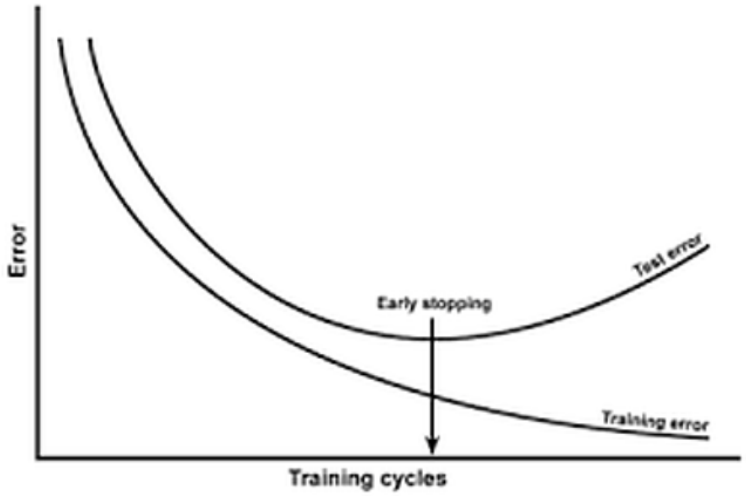

Figure 3.11. Schematic sketch early stopping explanation, Sagar (2019).

As shown in Figure 3.11, the training data still shows a decreasing trend while the test data is fading away in a parabolic way from the accuracy value.

3.5.3. Using of regularization

Regularization, like the other methods mentioned above, is a method to decrease the disorders of model. It takes place this by adding a penalty term to the loss function. The favorite used ones are are L1 and L2, Artem (2020).

L1 uses the absolute value. It is used for the purpose of minimizing the absolute value of the weights. The following Equation 3.8 explain L1 function.

$$L(x, y) = \sum_{i=1}^{n} \left(y_i - b_0\right)\left(x_i\right)^2 + \lambda \sum_{i=1}^{n} \left|w_i\right| \tag{3.8}$$

Where λ is normalized weights, L is loss, is predicted value, and b is bias. L2 tries to minimize the weights as L1. But it makes this by minimizing its square shown in Equation 3.9.

$$L(x, y) = \sum_{i=1}^{n} \left(y_i - b_\theta\right)\left(x_i\right)^2 + \lambda \sum_{i=1}^{n} w_i^{\,2} \tag{3.9}$$

Both regularization strategies are compared in the table below.

Table 3.2. Comparison of L1 and L2, Sagar (2019).

L1 Regularization	L2 Regularization
L1 disciplines the total of the absolute weight values.	Sum of square values of weights are disciplined by L2.
L1 creates a straightforward, comprehensible model.	Complex data patterns can be learned via L2 regularization.
L1 is more stamina to outliers	L2 is not as stamina as L1

L2 is better at analyzing more complex data. It is superior in terms of learning adaptation. It is more convenient to use L1 in solving simple linear problems as shown in Table 2.1.

3.5.4. Using of dropouts

The dropout method is one of the frequently used methods to prevent overfitting like other methods. For example, while L1 and L2 regulations prevent overfitting by changing the loss function, the dropout method achieves this by changing the network itself. It removes randomly selected neurons while training each iteration shown in Figure 3.12. Removing each neuron from the network will result in a different model. Thus, each dropout will make the overfitting decrease, Artem (2020).

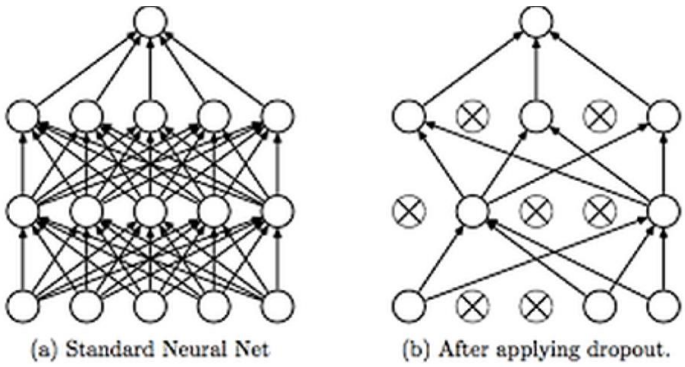

Figure 3.12. Schematic sketch of dropouts method before and after applying to the sample model, Sagar (2019).

4. MATERIALS AND METHODS

The methods of MLP and Eureqa GA, which will be used in the solution of the CO_2 heat transfer coefficient problem, are briefly explained below.

4.1. Multilayer Perceptron

This is the method used in the thesis. Therefore, it will be explained in more detail than the others. Multilayer perceptron is a feedforward artificial neural network. As in classical neural networks, an output is obtained by entering inputs between the layers. A neural network is formed by connecting many input and output layers. It performs the deep learning process using backpropagation.

The multilayer back propagation neural network method is mainly used in non-linear face recognition and image recognition problems. Its most obvious advantage is that it approaches the solution through backpropagation and is superior in solving complex problems. The multilayer perception method has inputs, hidden layers, and outputs. The result is obtained according to the transfer function selected according to the type of problem.

As aforementioned, neural networks with a single node are called perceptrons shown in Figure 4.1. The sensor consists of inputs such as x_1, x_2, x_3.....x_n and their w_1, w_2, w_3,.....w_n weights. The specified activation function uses these inputs afterward, multiplies them by weights, and produces the output.

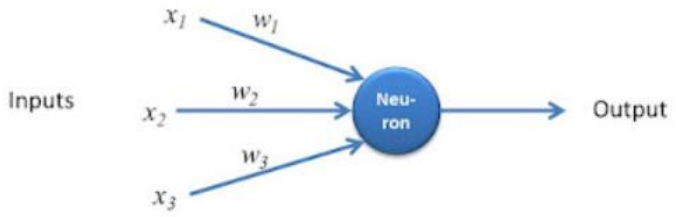

Figure 4.1. Schematic sketch **s**ingle layer perceptron**,** Phil (2017).

The most crucial point here is that multilayer perceptron networks should have at least three nodes. In addition to that, each neural node uses a nonlinear activation function except for entered inputs. As mentioned in the previous sections, the activation function transfers the inputs to the neuron by adding biases and weights. There are many activation

functions. Their usage depends on the type of problem and requires experience.

For example, there are many different types of activation functions such as RELU, TANH, SIGMOID etc. shown in Figure 4.2.

Activation function	Equation	Example	1D Graph
Linear	$\phi(z) = z$	Adaline, linear regression	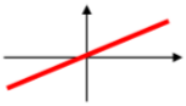
Logistic (sigmoid)	$\phi(z) = \frac{1}{1 + e^{-z}}$	Logistic regression, Multi-layer NN	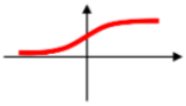
Hyperbolic tangent (Tanh)	$\phi(z) = \frac{e^{z} - e^{-z}}{e^{z} + e^{-z}}$	Multi-layer Neural Networks	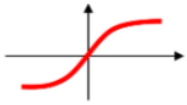
Rectifier, ReLU (Rectified Linear Unit)	$\phi(z) = max(0, z)$	Multi-layer Neural Networks	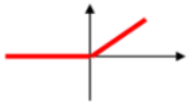

Figure 4.2. Activation function samples, Dosch (2021).

The selection of the transfer function is at the discretion of the researcher. The transfer function can be changed according to the expected result. Gradients and learning speed are controlled during the learning process. If there are inconsistencies during the process, the problem is solved by trying a different activation function. w is the weight vector. x is the input vector. b is the bias, and ϕ is the activation function. The output y would be given for the i_{th} neuron in equation 4.1.

$$y = \left(\sum_{i=1}^{n} w_i x_i + b \right) = \varphi\left(w^T x + b \right) \tag{4.1}$$

There should be at least three layers in an MLP. This rule is essential due to the requirement of at least one imperative hidden layer except for the input and output layers. This is illustrated in figure 4.3 below.

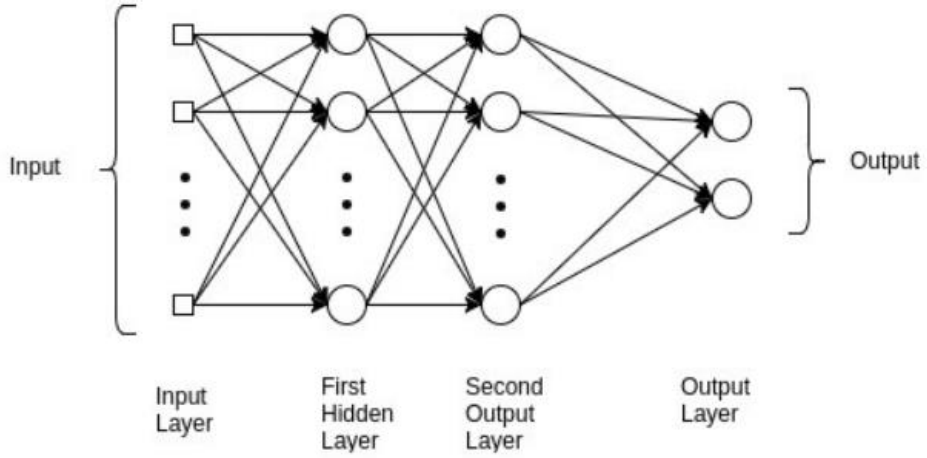

Figure 4.3. Schematic sketch of MLP, Peixoto (2020).

4.2. Introduction of GA

The well-known theory of natural selection is a structure that somehow exists in nature. GA works on the same principle. Eliminates weak solutions for an identified problem and reveals strong ones. More precisely, GA work like a laboratory test device rather than an artificial neural network program. While deriving experimental test results on the one hand, it tries to establish relationships between them on the other. Because while establishing the relationship, it operates by assigning it to a function or coefficient. This is precisely the crux of the matter.

As already explained in the literature review and the introduction, the main problem is that the two-phase flow boiling of CO_2 consists of complex factors, and a stable correlation cannot be established. The researchers tried to find solutions to existing correlations by assigning coefficients or functions. As a result, GA is a method that can be used to solve open-ended problems. Due to the many unpredictable or unsegregated data pollution, it is not straightforward to form an accurate model. For example, it is too tough to form a wise correlation or mathematical model for complicated multi-data problems. Dealing with these problems using classical artificial intelligence methods is challenging.

The advantage of GA is that they reduce complexity and produce models closer to actual conditions. We come across an algorithm that creates the most suitable model according to the available data. In addition, certain parts of the model can be developed locally by increasing prior knowledge. Once the data is properly prepared, GA calculates and reveals

which data are outliers and should be discarded and which data should be normalized or scaled. As it is known, optimization makes a process work better by using the best inputs to get the best results. This is essential for creating efficient working systems. For example, this is inevitable in energy and industrial applications. GA is perfect for obtaining a result by changing the input factors, more precisely by adding certain functions and coefficients.



Figure 4.4. Schematic sketch GA working principle, Michalewicz (1990).

4.2.1. Failure of gradient-based methods

Numerical methods or ANN methods have been used while solving complex problems due to the inability of traditional mathematical methods. A highly accurate model is identified related to thesis topic using the MLP artificial neural network. ANN methods can be overfitting in reasonably complex systems, which generally try to find solutions with the descent gradient logic. Observing overfit cases are tricky because of possible unsegregated inputs can still exist. For example, the process proceeds to the peakiest point by commencing derivation from any curve point in the gradient descent methods. However, this is challenging to achieve for a curve consisting of many independent peaks as shown in Figure 4.5.

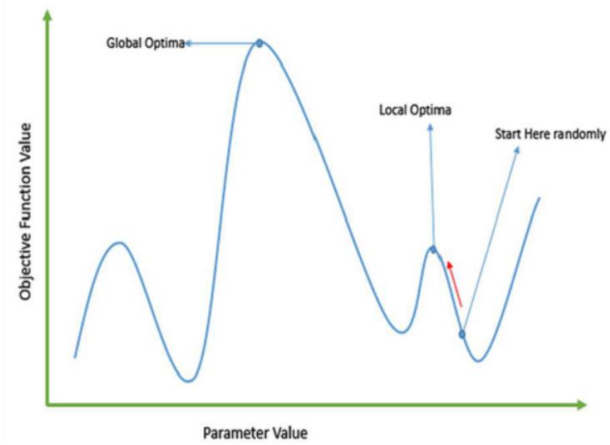

Figure 4.5. Figure of failure gradient-based methods**,** Michalewicz (1990).

4.2.2. Genetic algorithms fundamentals

The terms below define what GA is.

- Population: It is a batch of all the potential responses to the problem. A GA's population has human-like characteristics.
- Chromosomes: A chromosome is an arbitrary response to a problem.
- Gene: The gene is a component of the chromosome.
- Allele: An allele is a gene's value for a particular chromosome.

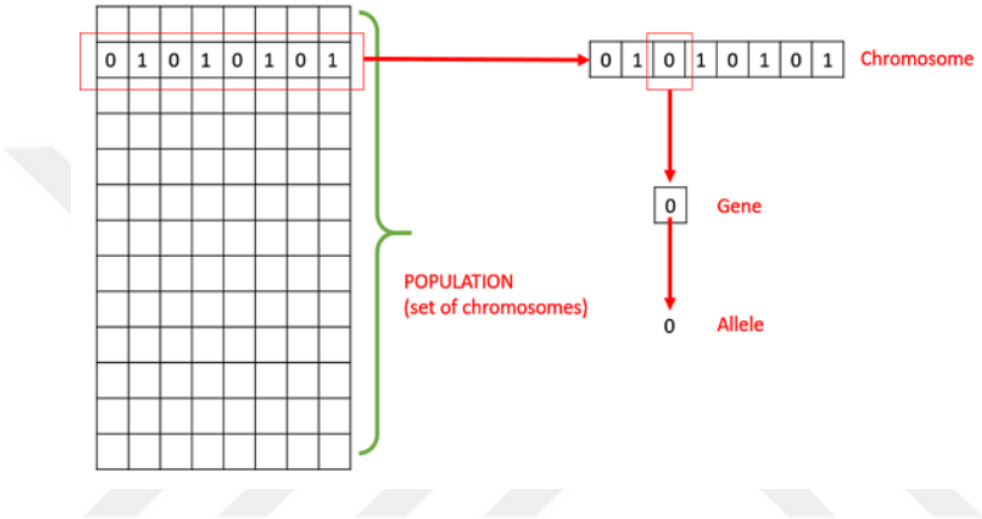

Figure 4.6. GA elements, Michalewicz (1990).

- **Genotype**: Genotype represents the population in the computational space. Solutions in the computational space can be manipulated very promptly and intelligently by means of estimation programs.
- **Phenotype**: Phenotypes are populations generated in real-world space. They represent the situation in real-world space.
- **Decoding and Encoding**: The phenotypic and genotype spaces are often the same in simple cases, but in complicated ones, the roles can be inverted. By converting from genotype to phenotype, decoding is accomplished. By changing the solution from phenotypic to genotype space, coding is performed. Decoding must be completed as soon as possible because it is used repeatedly in a GA during the determination of the fitness value.

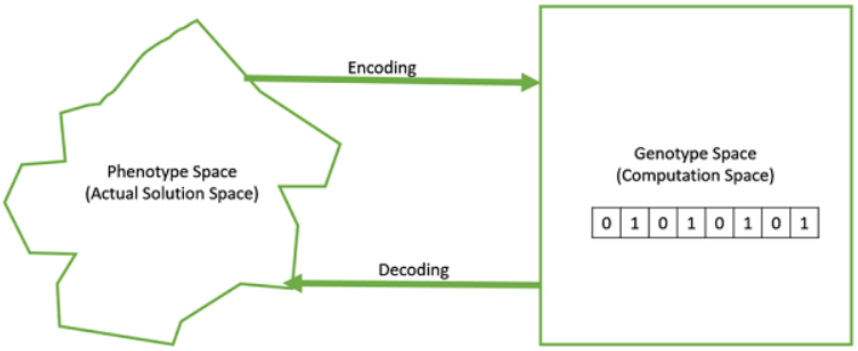

Figure 4.7. Schematic sketch GA elements, Michalewicz (1990).

- **Fitness Function:** To simply define the fitness function, it is something like that produces an appropriate result by taking an output and using it as an input. Although, it varies depends on the problem either the fitness or objective functions can be same or different.
- **Genetic operators:** These alter the offspring's genetic makeup. These include selection, mutation, and crossover.

A GA's fundamental framework begins with a population that is drawn at random. Parents are then chosen for a merger after that phase. To produce new offspring, crossover and mutation operations on the parents must be carried out. Finally, as shown in Figure 4.8, these offspring replace the existing members of the population, and the cycle resumes. In order to develop and find a solution, genetic algorithms attempt to mimic the human neurological system.

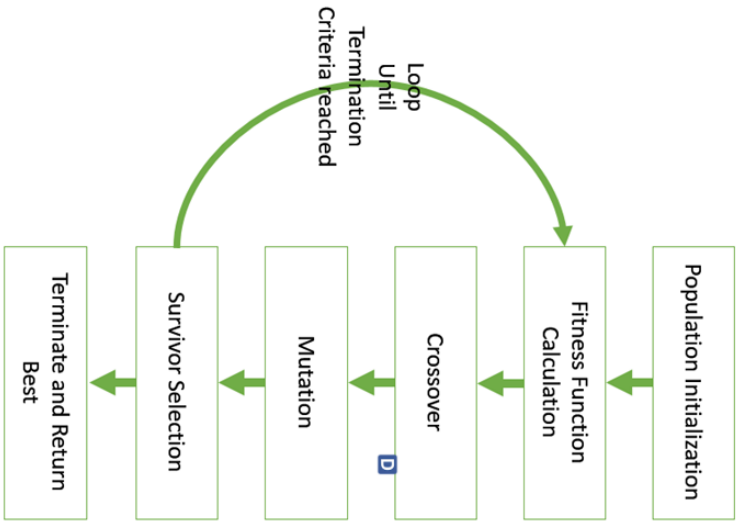

Figure 4.8. The basic structure of GA, Michalewicz (1990).

It is required to understand the following words related to Eureqa before beginning to interpret the model.

Sensitivity: The degree to which a variable in model has an effect on the target variable.

% Positive: The possibility that raising the target variable will also boost this one. If 70%, then 70% of time, increases in this variable result in increases in the target variable, while 30% of the time, it either decreases it or has no effect. Increases in this variable won't affect the target variable if % positive=0%.

Positive Magnitude: This is typically how much of a positive impact there is when increases in this variable cause a rise in the target variable.

% Negative: The probability that raising this variable will bring down the desired variable. If % negative=60, then increases in this variable result in declines in the target variable 60% of the time, while it has no effect 40% of the time. Increases in this variable will not cause the target variable to drop if % negative=0.

Negative Magnitude: This is typically how substantial the negative impact is when increases in this variable result in drops in the target variable.

Details: Given a model equation of the form z=f (x, y …….), the influence metrics of x on z are defined as follows:

Sensitivity: $\overline{\left|\frac{\partial z}{\partial x}\right|} \cdot \frac{\sigma(x)}{\sigma(z)}$, evaluated at all input data points.

%Positive: The percent of data points where $\frac{\partial z}{\partial x} > 0$

% Negative: The number of the data points where $\frac{\partial z}{\partial x} < 0$

Positive Magnitude: $\overline{\left|\frac{\partial z}{\partial x}\right|} \cdot \frac{\sigma(x)}{\sigma(z)}$, at all points where $\frac{\partial z}{\partial x} > 0$

Negative Magnitude: $\overline{\left|\frac{\partial z}{\partial x}\right|} \cdot \frac{\sigma(x)}{\sigma(z)}$, at all points where $\frac{\partial z}{\partial x} < 0$

Where:

$\frac{\partial z}{\partial x}$ is the partial derivative of z with respect to x,

$\sigma(x)$ is the standart deviation of x in the input data,

$\sigma(z)$ is the standart deviation of z,

$|x|$ denotes the absolute value of x

$\overline{x}$ denotes the mean of x

GA complexity: With respect to the number of generations, population size, and individual size, GA complexity is O(g(nm + nm + n)). The complexity is, therefore, on the order of O(gnm)). Because of this, the fitness function, which depends on the application, is being ignored.

Since the existing classical correlations could not give high-accuracy results, different methods were sought. One of them was the MLP multi-perceptron. It was worked out with three separate MLP models using Colab Tensor Flow Notebook within separate transfer functions as RELU and TANH, respectively. As the name suggests, the weights and inputs are created as vectors and quickly converted to tensors, and a solution is obtained.

Tensor flow classically uses Python, Pandas, and Numpy libraries. Code writing is the same as Python. The advantage is that it goes to the solution very quickly. The tensor flow can solve calculations that would take days with other programs in minutes. In order to develop an optimum architecture depends on many factors such as the number of inputs, number of training, regularization factor, and loss function factor. Too many hidden neural network layers can cause overfit with meaningless results. In addition, the lack of hidden layers and inputs negatively affects and restricts the deep learning function. Therefore, it was performed according to experience and knowledge and tried to create the most optimal model.

Consequently, a high-accuracy solution was obtained and presented as a MAPE with the MLP and GA methods as described literature studies. Twenty-six inputs have been used within the Colab Tensor flow notebook. While solving the heat transfer coefficient, 1017 experimental data were logged in models. Minimum and maximum pipe diameter ranges are taken between 1.4mm and 11.20mm. Minimum and maximum mass flow ranges were taken between 40kg/m^{2}s and 800kg/m^{2}s. Minimum and maximum saturation temperature ranges are taken between 243K and 288K. Minimum and maximum heat flow ranges are taken between 2kW/m^2 and 40kW/m^2. Lastly, a new correlation is produced by using Eureqa GA.

5. RESULTS AND DISCUSSIONS

The coding is written in Python software. Pandas and Numpy were used as libraries. Factors are assigned randomly in our study, as shown in Table 5.1. The experimental data set was split into training, test datasets, and validation datasets, with a split ratio of training data points, test data points, and validation data points.

The definitions assigned to the model are shown in table 5.1. The λ value was taken as 0.002. It can also be started with higher learning rates. A higher learning rate provides a fast approach to the target, but deviations may increase during converging to the target value. As mentioned earlier, overfitting should be avoided. In this regard, one of the regularization factors should be used. Here, the L2 factor is taken as 0.001. Adam is selected as adaptive optimization, but this is not binding. Optionally, the standard gradient descent algorithm can also be used. Since Adam's adaptive learning is better, it was preferred here.

Table 5.1. General factors of models

Factor	Value
Activitation Function	TANH, SIGMOID
L2 Regularization factor, α	0.001
Solver	ADAM
Batch Size	31
Epochs	1000
Learning Rate λ	0.002

Mean square error is generally used for that kind of problem defined in equation 5.1.

$$\text{MAPE}(\%) = 100 \times \frac{\sum_{k=1}^{n} n \left| \frac{h_{tp,exp} - h_{tp,pred}}{h_{tp,exp}} \right|}{n} \qquad \textbf{(5.1)}$$

$h_{tp,pred}$: Predicted output

$h_{tp,exp}$: Experimental output

n: Total number of observation

R^2 is preferred to R (Pearson's correlation coefficient). The main reason is that R estimates the linear correlation coefficient, whereas R^2 is entirely independent of the scaled dependent variable. Therefore, adaptation can be performed easier rather than R.

R^2 is defined in equation 5.2 below.

$$R^2 = 1 - \frac{\sum (h_{tp,exp} - h_{tp,pred})^2}{\sum (h_{tp,exp} - \bar{h}_{tp,pred})^2} \quad \textbf{(5.2)}$$

MLP model has been performed using Colab Tensor Flow. Colab is the IOE with Jupyter notebcad, Tensor Flow is a library in Keras.

5.1. MLP Neural Network Model 1

While creating the model, 26 variables and one output were used. Layers are set to the number of 10. The architecture of neurons in the layers was determined as 400,300, 220, 152, 100, 65, 60, 20, 10, and 1, respectively defined in Figure 5.1. While solving the heat transfer coefficient, 1017 experimental data were applied in models. Minimum and maximum D_{mm} ranges are taken between 1.4mm and 11.20mm. Minimum and maximum G ranges were taken between 40kg/m^{2}s and 800kg/m^{2}s. Minimum and maximum T_s ranges are between 243K and 288K. Minimum and maximum Q ranges are between 2kW/m^2 and 40 kW/m^2.

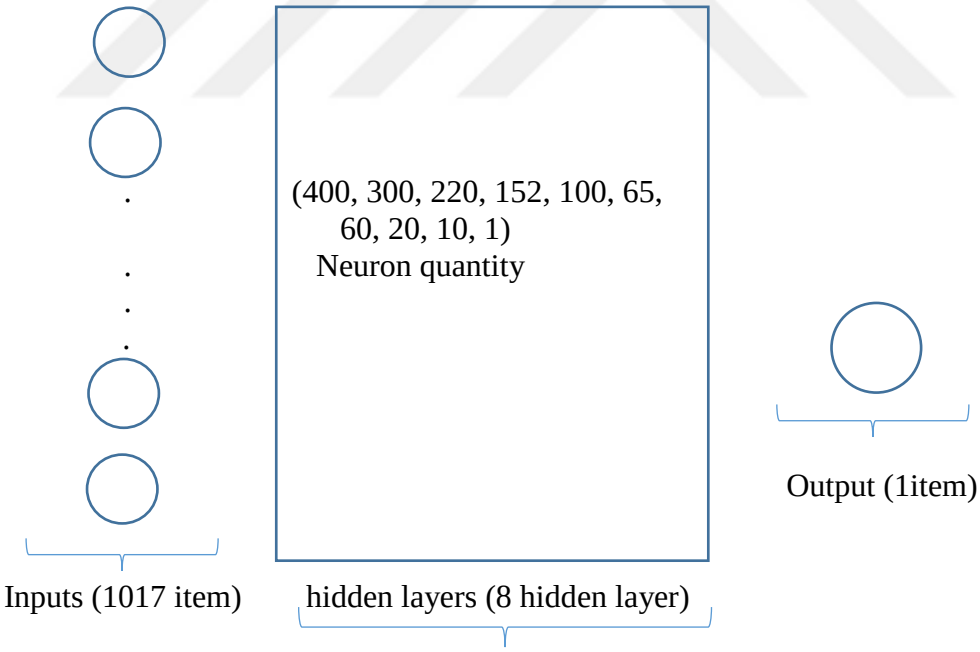

Figure 5.1. Architecture of Model1.

Many experimental studies have been made to determine the number of hidden layers and to select the optimum efficient neurons to prevent overfitting. The L2 optimization method was used to prevent overfitting. In order to make the model better, dropbox was

also done at each layer, reducing neurons randomly. Results were obtained as being 0.30 MAPE and 0.58 R^2 values for TANH, and 0.39 MAPE and 0.52 R^2 for SIGMOID function. These two value shows that our model predicts parallel. Unfortunately, the model did not yield a remarkably accurate output value for this model, as shown in Table 5.2.

Table 5.2. Results of MLP Model1.

Test Case ANN Model (400,300,220,152,100,65,60,20,10,1)	MAPE (%)		R^2	
	TANH	SIGMOID	TANH	SIGMOID
Inputs: D, x , G [kg/ms^2], Q [kW/m^2], T_{sat} [K] , $\frac{p_{total}}{p_{critic}} = p_r$, p_{total}, $\mu_l[kg/ms]$, $\mu_V[kg/ms]$, $c_{pl}[KJ/kgK]$, $c_{pv}[KJ/kgK]$, $k_l[KW/mK]$, $k_V[kW/mK]$, $\rho_l[kg/m^3]$, $\rho_V[kg/m^3]$, $\sigma[kg/m]$, Bo, Wb_l, Wb_v, X_{tt}, Re_v, Re_l, Fr_l, Pr_l, Pr_v, $\in$, A_L	30	39	0.58	0.52

5.2. MLP Neural Network Model 2

While creating the model, 26 variables and one output were used. Layers are set to the number of 10. It is tested with new segregated inputs which is over than 3mm diameter and lower than 273K. The new actual experimental inputs consist of 664 item. Three hundred fifty-three of them were segregated to achieve a smooth model. Manual segregation is performed in the study for outlier inputs. D_{mm} were chosen between 3.5-11.2mm, G value between 40-424 kg/m^{2}s, and Q kW/m^2 in the range of 4.94-20. T_s is chosen in the range of 243-273K. The architecture of neurons in the layers was determined as 500,350, 250, 150, 40, 30, 20, 10, 5, and 1, respectively shown in Figure 5.2. The MAPE accuracy value is around 0.24, and the R^2 value is observed as, 0.81 as shown in Table 5.3 obtained with TANH. The MAPE accuracy value is around 0.26, and the R^2 value is observed as, 0.78 as shown in Table 5.3 obtained for SIGMOID function.

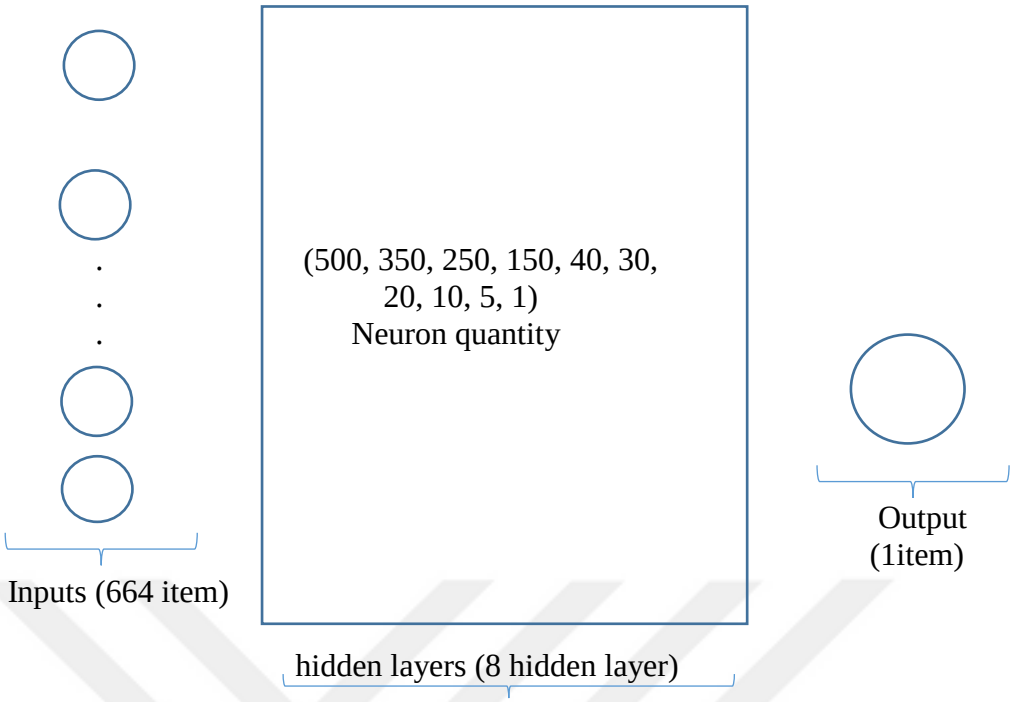

Figure 5.2. Architecture of Model 2.

Table 5.3. Results of MLP Model 2.

Test Case ANN Model (500,350,250,150,40,30,20,10,5,1)	MAPE (%)		R^2	
	TANH	SIGMOID	TANH	SIGMOID
Inputs: D, x , G [kg/ms^2], Q [kW/m^2], T_{sat} [K] , $\frac{p_{total}}{p_{critic}} = p_r$, p_{total}, $\mu_l[kg/ms]$, $\mu_v[kg/ms]$, $c_{pl}[KJ/kgK]$, $c_{pv}[KJ/kgK]$, $k_l[KW/mK]$, $k_v[kW/mK]$, $\rho_l[kg/m^3]$, $\rho_v[kg/m^3]$, $\sigma[kg/m]$, Bo, Wb_l, Wb_v, X_{tt}, Re_v, Re_l, Fr_l, Pr_l, Pr_v, $\in$, A_L	24	26	0.81	0.78

5.3. Eureqa GA Model

While creating the model, 26 variables and one output were used. The actual experimental inputs consist of 664 inputs which are same values with Model 2. D_{mm} below 3.5mm and saturation temperatures (T_s) above 273K were removed. Manual segregation was

performed in the study for outlier inputs. D_{mm} were chosen between 3.5-11.2mm, G value between 40-424 kg/m^{2}s, and Q kW/m^2 in the range of 4.94-20. T_s is chosen in range of 243-273K.The MAPE accuracy value is around 0.22, and the R^2 value is observed as being 0.985 as shown in Table 5.4. The study covers all patterns of two-phase flow boiling, including the mist flow region. The complexity is 39, as shown in Figure 5.3.

Best Solutions of Different Sizes

Size	Fit	Solution
39	0.162	$htc = 12 + \frac{-17.6}{Q} + 0.152\,Bo\,Rev - 7.26\,E - 28.7\,Rev\,E - 4.14\text{e-}9\,Wep^2 - 0.000918\,G\,Q\sin(Bo)$
37	0.165	$htc = 12.6 + \frac{-17}{Q} + 0.152\,Bo\,Rev - 7.99\,E - 29\,Rev - 4.01\text{e-}9\,Wep^2 - 0.000965\,G\,Q\sin(Bo)$
35	0.180	$htc = 11.6 + \frac{-16.2}{Q} + 0.000157\,Rev\,Bo^2 - 6.76\,E - 3.7\text{e-}9\,Wep^2 - 0.00104\,G\,Q\sin(Bo)$
34	0.199	$htc = 0.27\,Q + 0.00574\,Bo + 0.0917\,Bo\,Rev - 2.76\,x - 3.84\text{e-}9\,Wep^2 - 0.000661\,G\,Q\sin(Bo)$
33	0.201	$htc = 7.6 + \frac{-15.4}{Q} + 0.0908\,cpv\,Bo\,Rev - 0.00016\,Wep - 4.09\,x - 0.000963\,G\,Q\sin(Bo)$
32	0.206	$htc = 12.6 + \frac{-17.4}{Q} + 0.161\,Bo\,Rev + 0.000656\,G\,Q - 7.96\,E - 32.1\,Rev - 4.14\text{e-}9\,Wep^2$
30	0.218	$htc = 5.44 + 0.00397\,Bo + \frac{-15.5}{Q} + 0.118\,Bo\,Rev + 0.000818\,G\,Q - 0.000187\,Wep - 3.55\,x$
29	0.225	$htc = 0.267\,Q + 0.00596\,Bo + 0.0918\,Bo\,Rev + 0.000469\,G\,Q - 2.85\,x - 3.96\text{e-}9\,Wep^2$
28	0.228	$htc = 7.14 + \frac{-13.6}{Q} + 0.121\,Bo\,Rev + 2.05\text{e-}6\,G\,Q\,Bo - 0.000193\,Wep - 4.1\,x$
25	0.247	$htc = 0.328\,Q + 0.0125\,G + 0.00391\,Bo + 0.103\,Bo\,Rev - 0.000221\,Wep - 3.33\,x$
27	0.245	$htc = 0.343\,Q + 0.0138\,G + 0.00532\,Bo + 0.0899\,Bo\,Rev - 0.977 - 0.000214\,Wep - 2.88\,x$

Solution Details (calculated on validation data)

Solution	htc = 11.98 + -17.64/Q + 0.1517*Bo*Rev - 7.26*E - 28.72*Rev*E - 4.143e-9*Wep^2 - 0.000918*G*Q*sin(Bo)
R^2 Goodness of Fit	0.97105313
Correlation Coefficient	0.98544092
Maximum Error	1.0059314
Mean Squared Error	0.087416089
Mean Absolute Error	0.217196
Coefficients	7
Complexity	39

Figure 5.3. Best solutions of different complexities.

Table 5.4. Results of the Eureqa GA model.

Test Case Eureqa Algorithm Model	MAPE	R^2	Complexity
Inputs: D,x , G [kg/ms^2], Q [kW/m^2], T_{sat} [K] , $\frac{p_{total}}{p_{critic}} = p_r$, p_{total}, $\mu_l[kg/ms]$, $\mu_v[kg/ms]$, $c_{pl}[KJ/kgK]$, $c_{pv}[KJ/kgK]$, $k_l[KW/mK]$, $k_v[kW/mK]$, $\rho_l[kg/m^3]$, $\rho_v[kg/m^3]$, $\sigma[kg/m]$, Bo, Wb_l, Wb_v, X_{tt}, Re_v, Re_l, Fr_l, Pr_l, Pr_v, $\in$, A_L	0.22	0.985	39

The correlation obtained with the Eureqa GA optimization algorithm is shown in Equation 5.6. It can be seen solution of fit plots of train and validation data in Figure 5.4. It performs impressive graphics in terms of compatibility. GA algorithm segregated twenty inputs and just six input remained to set out correlation. Variable sensitivity results are shown in Table 5.5. As seen from the table, G, Q, and Re_v positively affect the result. ϵ and Bo have both negative and positive effects, and Wb_v has a negative effect on the result.

$$h_{tp} = 8.96 + 0.327Q - \frac{12.1}{Q} - \frac{19.6Q}{G} + 0.000157Re_v Bo^2 - 6.53e^{-5Wb_v} - 6.65 \in -2.22\sin(Bo) \quad \textbf{(5.6)}$$

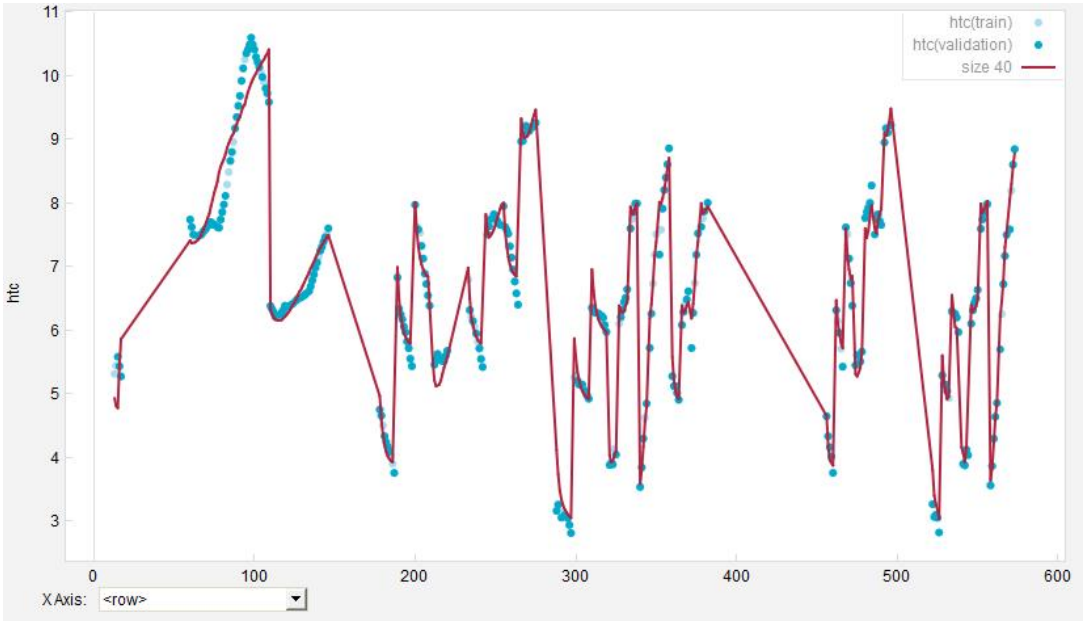

Figure 5.4. Solution fit plot.

It can be seen how much effect each factor has on the obtained correlation in Table 5.5.

Table 5.5. Variable Sensitivity Results.

Variable	Sensitivity	Positive %	Positive Magnitude	Negative %	Negative Magnitude
Bond Number (Bo)	2.8569	75 %	1.2306	25 %	7.7359
Heat Flow (Q)	0.80778	100 %	0.80778	0 %	0
Vapor Phase Reynold Number (Re_v)	0.69448	100 %	0.69448	0 %	0
Mass Flow (G)	0.43532	100 %	0.43532	0 %	0
Void Fraction (ϵ)	0.32834	100 %	0	100 %	0.32834
Vapor phase Weber Number (Wb_v)	0.19786	0 %	0	100 %	0.19786

5.3.1 Factor Analysis with R Studio

It was checked again with R studio to confirm the accuracy of the optimization and factor analysis applied with GA below. It is also proved that G, Q, Bo, We_p, Re_v, and ϵ inputs have an effect on the correlation as obtained GA algorithm defined in Table 5.6.

Table 5.6. R studio factor analysis results

Loadings

	Factor1	**Factor 2**	**Factor 3**	**Factor 4**	**Factor 5**
Htc	0.113	0.167	**0.938**	-0.255	0.363
X	**0.928**				0.363
G		**0.915**	0.202	-0.282	
Q			0.496		

Table 5.6. R studio factor analysis results **(continued)**

Bo		-0.118	-0.269	**0.818**	
We_p		**0.978**			
X_{tt}	-0.967				0.179
Re_v	0.571	**0.701**	0.134	0.205	0.161
€	**0.992**				

5.4. MLP Neural Network Model 3

Finally, to prove the accuracy of the 6-variable correlation obtained by GA, the MLP method was tried using the same variables and input of quantity (664). Thus, it is possible to comment on the accuracy of the obtained correlation. D_{mm} below 3.5mm and saturation temperatures (T_s) above 273K were removed. D_{mm} were chosen between 3.5-11.2mm, G value between 40-424 kg/m^2s, and Q kW/m^2 in the range between 4.94-20. T_s is chosen in range of 243-273K.The MAPE accuracy value is around 0.25, and the R^2 value is observed as, 0.80 for TANH, and MAPE accuracy value is around 0.29, and the R^2 value is observed as, 0.74 for SIGMOID function as shown in Table 5.7.

MLP model has been performed using Colab Tensor Flow Notebook. While creating the model, 6 inputs and one output were used. We set the number of layers to 10. The number of neurons in the layers was determined as 620, 380, 257, 150, 45, 30, 20, 10, 5, and 1 as shown in Figure 5.5.

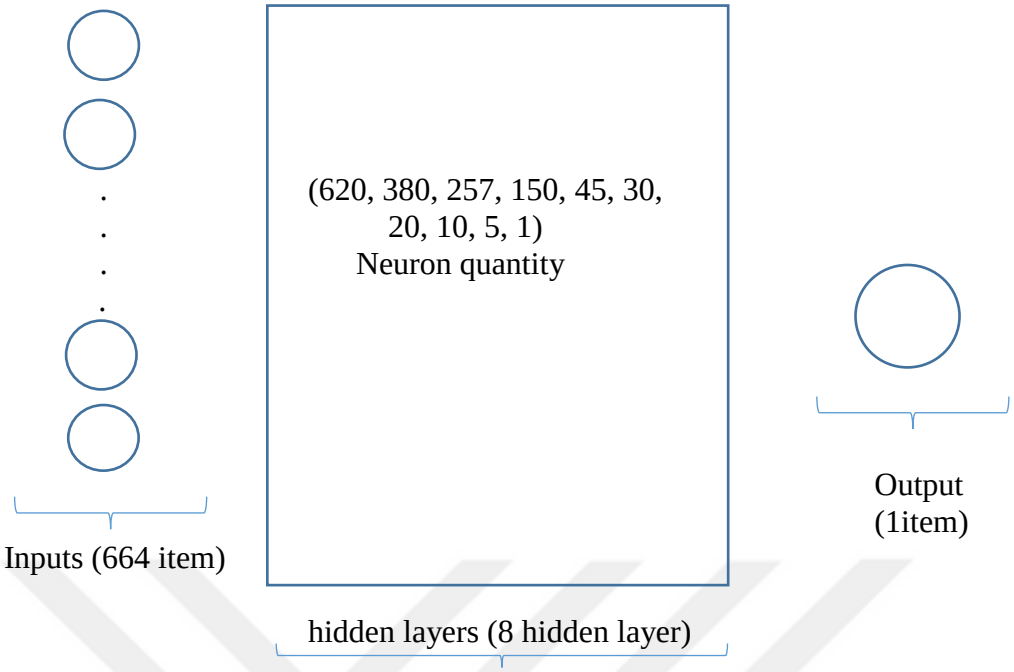

Figure 5.5. Architecture of Model3.

Table 5.7. Results of MLP model 3

Test Case ANN Model (620,380,257,150,45,30,20,10,5,1)	MAPE		R^2	
	TANH	SIGMOID	TANH	SIGMOID
Inputs: G [kg/ms^2], Q [kW/m^2], Bo,Wb_v, Re_v, ∈	0,25	0.29	0.80	0.74

5.5. Discussion

Due to the mathematical model's difficulty, many optional models are created in the MLP to get a highly accurate one. Dropbox method and L2 regularization were used to avoid overfitting results. As a result, it was determined that the MAPE results of models1, model2, and model3 which were formed in the tensor flow MLP method, differed from each other, once, functions are used as RELU and TANH, respectively. This indicates the complexity of the problem even though dropout and L2 regularization are used in the model.

The MAPE value did not yield a good result in the first MLP model. The MAPE value and R^2 value yielded better results after the diameters below 3mm and saturation temperatures over than 273K were segregated. In the last two MLP models, MAPE and

R^2 values have improved and obtained almost the same high accuracy rate.

Eureqa GA was used in the optimization and factor analysis process. Along with the segregation applied in the model, 424 outlier inputs are extracted. After segregation, a correlation was yielded. The Model R^2 has become more stable, and also MAPE has also become better as well. Only 6 variables remained in the factor analysis with GA. To prove this, factor analysis was performed again with R studio. As a result, the values were obtained very close to each other.

Eureqa GA produced an equation using only 6 of 26 variables according to the current experimental values. From the four different methods (3 MLP and one GA) shown in Table 5.8 used to solve the problem, the highest MAPE accurate rate was obtained with the GA after the segregation of outlier data. Since researchers show results distinctly in Table 5.10 as MAPE using classical methods, in the same way, Table 5.8 and Table 5.9 are prepared as MAPE based on the GA method to compare to different pipe diameters separately. Thome and Hajal (2004) present the best classical correlation at 248K as a 2.6% mean deviation error value provided before dry out. However, our correlation covers all patterns without restriction, especially relevant for 6mm diameter unless otherwise stated, including mist flow and dry flow regions. This proves the superiority of AI and GA over classical methods.

When the correlations in the literature are examined, it has been determined that the Wb_v (Vapor-Weber Number) input is not used in macro pipes over 3mm. Deviations from high accuracy may be due to missing inputs like Wb_v as shown equation 5.6.

In the factor analysis performed in R studio, the X_{tt} number was deliberately included in the analysis. As a result, it was seen that there was almost 100% negative effect on macro pipes. This confirms researchers such as Cooper (1984), Gungor, Winterton (1986), and Kandlikar (1990) who do not use X_{tt} in macro pipes.

It is determined that Bo (Bond number), Q (heat flux), and G (mass flux) have a significant positive effect on the correlation in comparison to the other factors, such as We_v (Weber number) and Re (Reynold number) shown being detailed in Table 5.5.

Table 5.8. Comparison of mean square error between applied methods.

Method	Inputs	MAPE %	R^2
Tensor Flow-MLP neural network model 1 using RELU Activitation Function	1017	30	0.58
Tensor Flow-MLP neural network model 2 using TANH Activitation Function	664	24	0.81
GA Eureqa Algorithm	664	22	0.98
Tensor Flow-MLP neural network model 3 using TANH Activitation Function	664	25	0.80

Table 5.9. Analysis of the heat transfer coefficients for expected flow boiling.

Data Used	Data Points	MAPE
D = 6 mm, G = 98-405 kg/m^2 s, T_{sat} = 243-273K, x=0.04-0.82 Q = 4.9-15.50 kW/m^2	346	13%
D = 7 mm, G = 200 kg/m^2 s, T_{sat} = 248-263K, x=0.14-0.95 Q = 6 kW/m^2	88	6%
D = 3.5 mm, G = 196-407 kg/m^2 s, T_{sat} = 243-258K, x=0.082-0.84 Q = 6 kW/m^2	51	17%
D =11.20 mm, G = 40-200 kg/m^2 s, T_{sat} = 243-258K, x=0.09-0.82 Q = 5-10 kW/m^2	99	75%
D =10 mm, G = 80 kg/m^2 s, T_{sat} = 245K, x=0.15-0.82 Q = 8 kW/m^2	30	64.7%

Table 5.10. Several empirical correlations for the estimation of CO_2 boiling heat transfer (before dryout).

Reference	Application Range	MAPE (%)		
		T_{sat} (K)		
		263K	248K	245K
Cooper (1984)	Nucleate boiling	53.7%	54%	5.2%
Jung et al. (1989)	Pure fluids and mixture	55%	42.3%	36.1%
Gungor and Winterton (1986)	vertical or horizontal tube $3.05mm \leq D_{mm} \leq 32.0mm$	40.1%	26.5%	7.0%
Liu and Winterton (1991)	$568.9 \leq Re_l \leq 8.75\times105$ $2.95mm \leq D \leq 32.0mm$ $0.83 \leq Pr_l \leq 9.1$	59.0%	54.5%	19.2%
Kandlikar (1990)	For vertical or horizontal tube with Fr_l	56.8%	42.9%	51.8%
Thome and Hajal (2004)	Special for CO_2 $248K \leq T_{sat} \leq 298K$ $0.79mm \leq D \leq 10.06mm$	21.8%	2.6%	48.3%

The accuracy of our model has been proven with three different applications with reference to the literature studies. The obtained correlation gives the best result between 6-7mm diameters, see Figures 5.6 and 5.7.

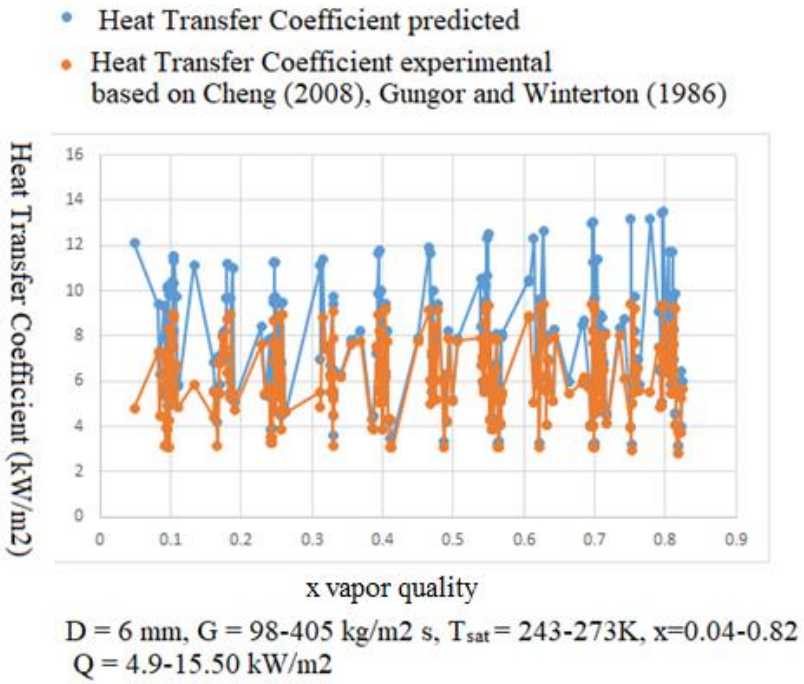

Figure 5.6. Heat transfer coefficient comparison for D = 6 mm, G = 98-405 kg/m^{2}s. T_{sat} = 243-273K, x=0.04-0.82, Q = 4.9-15.50 kW/m^2.

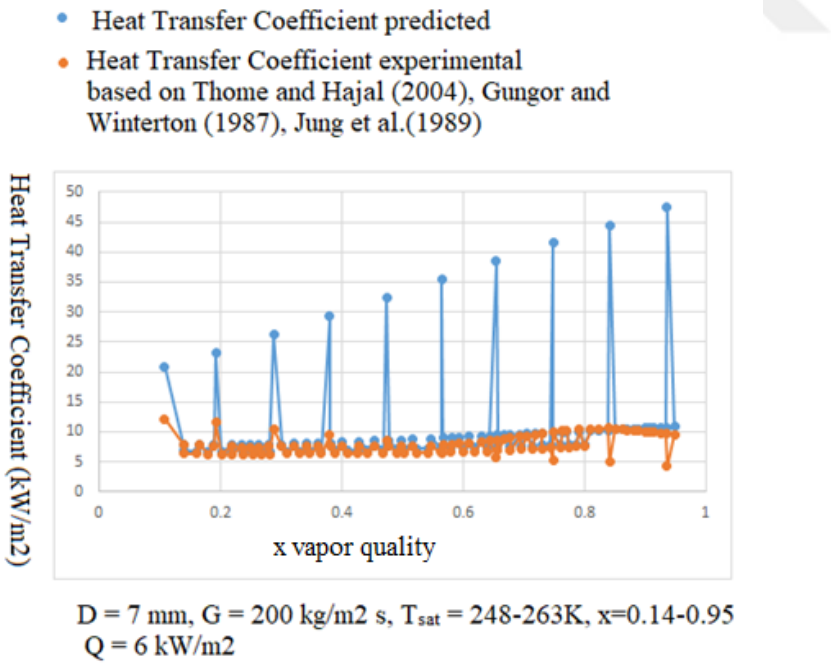

Figure 5.7. Heat transfer coefficient comparison for D = 7 mm, G = 200 kg/m^2 s, T_{sat} = 248-263K, x=0.14-0.95, Q = 6 kW/m^2.

The obtained correlation gives the worst result over the 10mm diameter range, see Figure 5.8 and Figure 5.9.

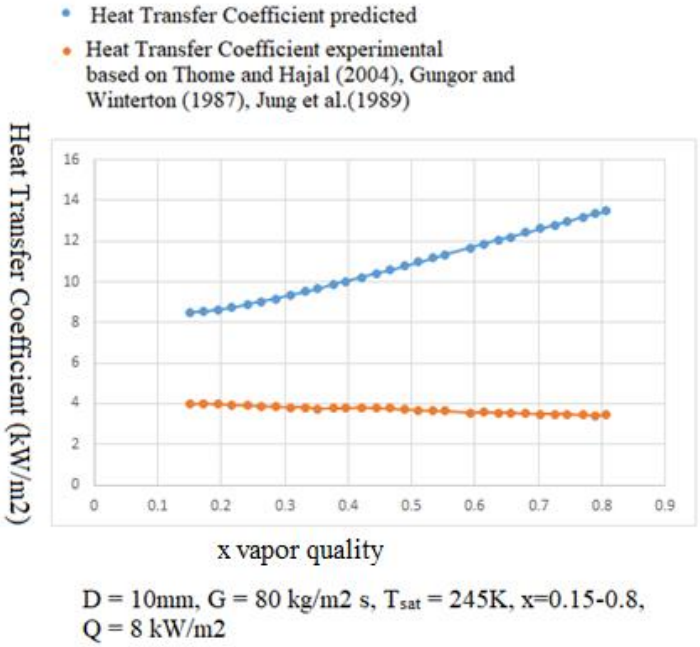

Figure 5.8. Heat transfer coefficient comparison for D =10 mm, G = 80 kg/m^2 s, T_{sat} = 245K, x=0.15-0.82, Q = 8 kW/m^2.

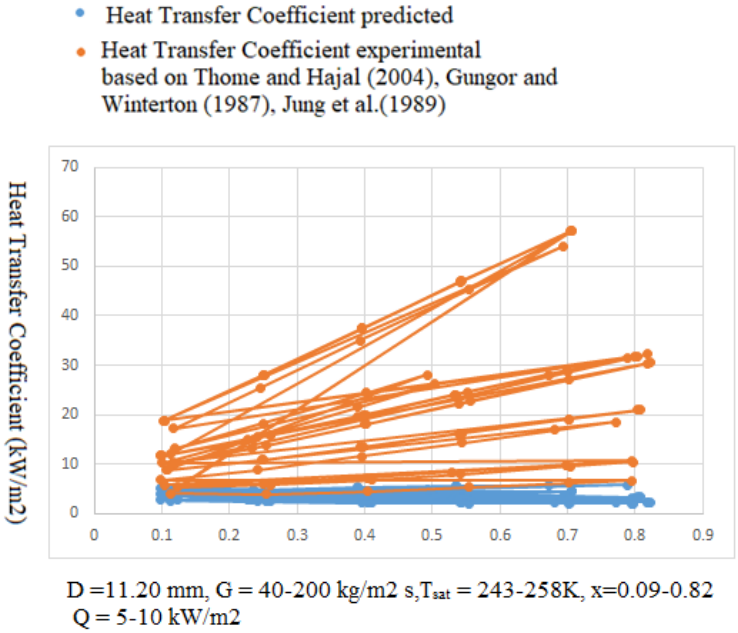

Figure 5.9. Heat transfer coefficient comparison for D =11.20 mm, G = 40-200 kg/m^2 s, T_{sat} = 243-258K, x=0.09-0.82, Q = 5-10 kW/m^2

The accuracy of the model was improved after the diameters extracted were smaller than 3mm from the 1017 inputs. This supports the research of Kandlikar (2002) that the macro channel diameters should be bigger than 3mm.

6. CONCLUSION

CO_2 showed different properties than other conventional gases due to its thermophysical properties. The saturation temperature of CO_2 is more effective on the heat transfer coefficient compared to other gases. Additionally, CO_2 has high critical pressure and low critical temperature. This causes restriction of usage as usual cooling gases. Eventually, it is well known that the CO_2 heat transfer coefficient shows the best performance in the nucleate region. However, none of these are applicable to CO_2 evaporation in horizontal pipes due to very high reduced pressures and low surface tensions of CO_2, which significantly affect the two-phase flow characteristics of CO_2.

This study analyzes the CO_2 two-phase flow boiling heat transfer coefficient using AI and GA methods instead of classical solution methods. Since the classical methods are scanty to yield a highly accurate solution contrary to contemporary methods, AI and GA are used for creating the new correlation.

Researchers obtained highly accurate results in bubbly, stratified, and intermittent flow regions using classical correlations except for mist and dry flow regions. Although the researchers developed their correlations by utilizing each other's studies, a highly accurate correlation covering all flow patterns could not be incorporated because there is still an open point to make tuning for a better correlation even though Cheng et al. (2006) have obtained highly successful solutions in other flow patterns such as intermitted, intermitted wavy, slug flow, etc. rather than mist flow and dry flow models. However, more studies and tests are required to establish a valid correlation in dry and mist flow pattern regions.

In this study, two MLP (multilayer perceptron) models are implemented, changing activation functions as RELU and TANH, respectively, using the Colab Tensor Flow tool notebook. It has obtained MAPE values of 0.30, 0.24, and 0.25 and a good fitness value of 0,58, 0.81, and 0.80 respectively. 26 variable and 1017 data are used to a make prediction in the model consisting of different 26 parameters.

Even though normalizing, dropbox and L2 regularization methods have been applied to improve the model and prevent overfitting. Despite all these efforts, the result was worse than expected in MLP method. However, the results showed that the data should be segregated. This proves the problem's complexity and is why no results can be obtained

with classical methods. In addition, it should be taken into account that some of the data obtained and compiled from different researchers may have measurement errors.

It has been decreased the number of layers along with the activation functions, but the accuracy of the Model has been almost unchanged. Afterward, the Model was optimized by Eureqa Genetic Algorithm after extracting 424 outlier data from the dataset. It was reduced from 26 variables to 6 variables by optimization and factor analysis with GA. To prove the accuracy of variables, the variables re-obtained by GA factor analysis. The factor analysis was performed again with R studio. The effect values of the variables showed almost similar characteristics. The accuracy of Model performed better results when diameters smaller than 3mm were extracted from a total of 1017 data. This supports the research of Kandlikar (2002) that the macro channel diameters should be bigger than 3mm. It was also proved that X_{tt} has negative effect on macro channels by the means of R Studio factor analysis, Hrnjak et al. (2007).

With the use of the GA optimization method, it has been obtained the best solution as 6% of MAPE with those data are in order D = 7 mm, G = 200 kg/m^{2}s, T_{sat} changes in the range 248-263K, and vapor quality value changes in the range 0.14-0.95. Nevertheless, Cheng et al. (2006) found a 30% MAPE in their study except in dry-out and mist flow regions for the diameters between 3-10mm.

The most interesting result among the factors that emerged in the correlation is We_v. Obviously, it was already known that mass flow, heat flux, Reynolds number, void fraction, and Bond number are effective on two-phase flow boiling for CO_2. However, there is no study in which We_v is used in any correlation for macro pipes bigger than 3mm. Actually, it was expected this result. Because the Weber number is a dimensionless factor arising from the relationship between inertia and the surface tensions in different phases that usually occur in two phase-flow boiling cases. It is frequently used during the formation of bubbly and film layers in liquids.

Nevertheless, the result of the optimization study shows that optimization has to recap with new experimental data due to reach high accuracy. This study should be done with AI and GA parallel to test the equipment system to validate the results. It is very peculiar to obtain different heat transfer coefficient values under identical test conditions. It is tough to explain this situation from the thermophysical properties perspective. The reason can be insufficient

precise sensitivity of the measuring devices or incomplete or inaccurate measurement factors. For these reasons, more precise measurements should be made using sensitive and calibrated test equipment and tools.

REFERENCES

Articles:

Bansal, P.K, Zhao, X. (2010) Flow boiling heat transfer of CO_2 at low temperatures – a critical review Department of Mechanical Engineering, The University of Auckland Private Bag 92019, Auckland, New Zealand.

Bredesen A.M, Hafner A. H, Pettersen J, Neksa P and Aflekt K. 1997, Heat transfer and pressure drop for in-tube evaporation of CO_2, Proc. IIF/IIR: 35-49.

Cheng, L., Ribatski, G., Thome, J. R. (2008) "New prediction methods for CO_2 evaporation inside tubes: Part II - A general flow boiling heat transfer model based on flow patterns," Int. J. Heat Mass Transfer, vol. 51, pp. 125-135.

Cheng, L., Ribatski, G., Wotjan, L., Thome, J. R. (2006) New flow boiling heat transfer model and flow pattern map for carbon dioxide evaporating inside horizontal tubes, a Laboratory of Heat and Mass Transfer (LTCM), Faculty of Engineering Science (STI), E´ cole Polytechnique Fe´de´rale de Lausanne (EPFL), CH-1015 Lausanne, Switzerland b Institute of Process Engineering, University of Hannover, Callinstraße 36, 30167 Hannover, Germany.

Cooper, M. G. (1984) "Saturation nucleate pool boiling: a simple correlation," in 1st U.K. National Conference on Heat Transfer, vol. 2, pp. 785-793.
Dennis, Y.C.L., Giorgio, C.M., Mercedes, M.V. (2014). An overview of current status of carbon dioxide capture and storage technologies, Volume 39, Pages 426-443

Dittus, F. W, Boelter, L. M. K. (1930) "Heat transfer in automobile radiator of the annular type," Univ. Calif. Publ. Eng., vol. 2, pp. 443-461.

Friedel L.: Improved friction pressure drop correlations for horizontal and vertical two-phase pipe flow European Two-Phase Flow Group Meeting, E2, Ispra 1979.

Gungor, K.E., Winterton, H.S. (1987) Simplified general correlation for saturated flow boiling and comparisons of correlations with data, Chem. Eng. Res. Des. 65 (1987) 148–156.

Jung, D.S., McLinden, M., Radermacher, R., Didion, D. (1989) A study of flow boiling heat transfer with refrigerant mixtures, Int. J. Mass Transfer 32 (9) (1989) 1751– 1764.

Kandlikar S.G. 1990, A general correlation for saturated two-phase flow boiling horizontal and vertical tubes, Trans. ASME. 112: 219-228.

Kandlikar, S.G (2002) "Fundamental issues related to flow boiling in minichannels and microchannels," Exp. Therm. Fluid Sci., vol. 26, pp. 389-407.

Kattan, N., Thome, J.R., Favrat, D. (1998) "Flow boiling in horizontal tubes. Part 1:

Development of a diabatic two-phase flow pattern map," J. Heat Transfer, vol. 120, pp. 140-147.

Kattan, N., Thome, J.R., Favrat, D. (1998): "Flow boiling in horizontal tubes: Part-3: Development of a new heat transfer model based on flow patterns," J. Heat Transfer, vol. 120, pp. 156-165.

Kattan, N., Thome, J.R., Favrat, D. (1998): Part 2-New heat transfer data for five refrigerants," J. Heat Transfer, vol. 120, pp. 148-155.

Liu, Z., Winterton, R.H.S. (1991) A general correlation for saturated and subcooled flow boiling in tube and annuli, based on a nucleate pool boiling equation, Int. J. Heat Mass transfer. 34(11): 2759- 2766.

Lunda, L., Aursanb, P. (2014) Two-Phase Flow of CO_2 with Phase Transfer Dept. of Energy and Process Engineering, Norwegian University of Science and Technology (NTNU), NO-7491 Trondheim, Norway bSINTEF Energy Research, Sem Sælands vei 11, NO-7465 Trondheim, Norway

Maina, P., Huan, Z. (2015) A review of carbon dioxide as a refrigerant in refrigeration technology, Department of Mechanical Engineering, Tshwane University of Technology, Private Bag X680, Pretoria 0001, South Africa, pp.10.

Mikielewicz, D., Jakubowska, B. (2016) Prediction of flow boiling heat transfer coefficient for carbon dioxide in minichannels and conventional channels, Gdansk University of Technology, Faculty of Mechanical Engineering, Department of Energy and Industrial Apparatus, Narutowicza 11/12, 80-233 Gdańsk, Poland.

Müller-Steinhagen R., Heck K.: A simple friction pressure drop correlation for twophase flow in pipes. Chem. Eng. Process. 20(1986), 6, 297–308.

Oh, J.T, Pamitran, A.S., Choi K.I., Hrnjak, P. (2011) Experimental investigation on two-phase flow boiling heat transfer of five refrigerants in horizontal small tubes of 0.5, 1.5 and 3.0 mm inner diameters, Int J Heat Mass Trans, 54; 2011:2080-2088.

Peixoto, F. (2020). A Simple overview of Multilayer Perceptron(MLP). Published On December 13, 2020 and Last Modified On December 18th, 2020.

Sagar, A. (2019) 5 Techniques to Prevent Overfitting in Neural Networks, VIT Vellore on December 6, 2019 in Neural Networks, Overfitting.

Shah, M.M. (1988) Chart correlation for saturated boiling heat transfer: equations and further study, ASHRAE Trans.2673 185–196.

Sun, F., Xie, G., Li, S. (2021) An artificial-neural-network based prediction of heat transfer behaviors for in-tube supercritical CO_2 flow School of Mechanical Engineering, Northwestern Polytechnical University, Xi'an, 710072, China School of Marine Science and Technology, Northwestern Polytechnical University, Xi'an, 710072, China Research & Development Institute of Northwestern Polytechnical University in Shenzhen, Shenzhen, 518057, Guangdong, China.

Thome, J., Hajal, J.E. (2004) Flow boiling heat transfer to carbon dioxide: general prediction method, Int. J. Refrig. 27(3): 294-301.

Tran, T.N., Wambsganss, M.W., France, D.M. (1996) Small circular- and rectangularchannel boiling with two refrigerants, Int. J. Multiphase Flow 22 (3) (1996) 485–498

Wojtan, L., Ursenbacher, T., Thome, J. R. (2005) Investigation of flow boiling in horizontal tubes: Part I – A new diabatic two-phase flow pattern map, Int. J. Heat Mass Transfer, vol. 48, pp. 2955-2969.

Yagov, V.V (2009) Heat transfer ın vapour-lıquıd flow of CO_2 Moscow Power Engineering Institute (Technical University), Krasnokazarmennaya, 14, 111250, Moscow, Russia

Yun, R., Kim, Y., Kim, M. S. (2005) "Convective boiling heat transfer characteristics of CO_2 in microchannels," Int. J. Heat Mass Transfer, vol. 48, pp. 235-242.

Conference:

Guimei, L., Zhezhao, Z. (2008). A Neural-Network Algorithm for Solving Nonlinear Equation Systems 2008 International Conference on Computational Intelligence and Security, 13-17 December, Suzhou, China.

Tiejun, Z., Saleh, M., Guanqiu, L. (2013) Fundamental Considerations for Designing Compact Solar Thermal Power and Ejector Cooling Systems in Hot Climates, Proceedings of the ASME 2013 International Mechanical Engineering Congress and Exposition IMECE2013 November 15-21, 2013, San Diego, California, USA

Book :

Ben, K., Patrick V. D.S (1996). An introduction to Neural Networks Eighth Edition, Institute of Robotics and System Dynamics German Aerospace Research Establishment P.O. Box 1116, D-82230 Wessling Germany

Hrnjak, P.S., Park, C.Y. (2007). CO_2 and R410a Flow Boiling Heat Transfer, Pressure Drop, and Flow Pattern in Horizontal Tubes at Low Temperatures, Air Conditioning and Refrigeration Center University of Illinois Department of Mechanical Science & Engineering 1206 West Green Street Prepared as part of ACRC Project #183 Urbana, IL 61801

Michalewicz, Z. (1996) Genetic Algorithms Data Structures Evolution Programs, Springer Berlin, Heidelberg 3th Edition, Berlin, Germany.

Osval, A., Montesinos ,L., Abelardo, M. L., Jose, C. (2022). Multivariate Statistical Machine Learning Methods for Genomic Prediction, pp 379–425

Phil, K. (2017). MATLAB Deep Learning With Machine Learning, Neural Networks and Artificial Intelligence, Seoul, Korea (Republic of) ISBN-13 (pbk): 978-1-4842-2844-9 ISBN-13 (electronic): 978-1-4842-2845-6 DOI 10.1007/978-1-4842-2845-6 Library of Congress Control Number: 2017944429.

Thanganadar, D., & Fornarelli, F., Camporeale, S., Asfand, F., Patchigolla, K. (2021). Off-design and annual performance analysis of supercritical carbon dioxide cycle with thermal storage for CSP application, Applied Energy, Elsevier, vol. 282(PA).

Thome, J.R. (2015). Encyclopedia of Two-Phase Heat Transfer and Flow I: Special Topics and Applications (A 4-Volume Set)

Electronic Publications :

Allam, Z. (2019) Achieving Neuroplasticity in Artificial Neural Networks through Smart Cities Curtin University Sustainability Policy Institute, Curtin University,Perth,WA6102, Australia Smart Cities 2019, 2(2),1184, http://doi.org/10.3390/smartcities2020009 Received :12 February 2019 / Revised : 8 March 2019 / Accepted : 2 April 2019 / Published : 8 April 2019.

Artem, O. (2020) Regularization in Deep Learning L1, L2, and Dropout, *Originally* published at https://www.deeplearning-academy.com.

Cavallini, A., Zilio, C. (2022). Carbon dioxide as a natural refrigerant, Dipartimento di Fisica Tecnica, University of Padova Via Venezia, 1 – I 35131 Padova PD, Italy https://academic.oup.com/ijlct/article/2/3/225/758001.

Dosch, B. (2021). ML Activation Functions.
https://medium.com/@BenDosch/ml-activation-functions-f851fd6334d2

Zulkifli H. (2019) Understanding Learning Rates and How It Improves Performance in Deep Learning
https://www.kdnuggets.com/2018/02/understanding-learning-rates-improves-performance-deep-learning.html

Kan, A. (2017). Multilayer Perceptron. Backpropagation COMP90051 Statistical Machine Learning, University of Melbourne,
https://trevorcohn.github.io/comp90051-2017/slides/07_backpropagation.pdf

Keerthana, V. (2021). Artificial Neural Network, Its inspiration and the Working Mechanism, Data Science Blogathon, https://www.analyticsvidhya.com/blog/2021/04/artificial-neural-network-its-inspiration-and-the-working-mechanism/

Liangxing, L., Haoxiang, Z., Jiayuan, Z., Xiangyu, L. (2022) Single/Multi-Objective Optimization Design and Numerical Studies for Lead-to-Supercritical Carbon Dioxide Heat Exchanger Based on Genetic Algorithm, Appl. Sci. 2022, 12, 7656, https://doi.org/ 10.3390/app12157656

Qi, H., Gui, N., Jiang, S. (2018) The application of supercritical CO2 in nuclear engineering: A review Volume 10, Issue 4,https://doi.org/10.1177/1757482X18765377

Takafumi Sasakawa, Jinglu Hu, Kotaro Hirasawa (2007). Wiley Periodicals, Inc. Electr Eng Jpn, 162(1): 32–39, 2008; Published online in Wiley InterScience, www.interscience.wiley.com, DOI 10.1002/eej.20600

Yang, M. (2016). Numerical Study on the Heat Transfer of Carbon Dioxide in Horizontal Straight Tubes under Supercritical Pressure PLoS One. 2016; 11(7): e0159602. Published online 2016 Jul 26. doi: 10.1371/journal.pone.0159602 https://www.ncbi.nlm.nih.gov/pmc/articles/PMC4961450/

APPENDICES

APPENDIX A : Correlations for conventional pipes (macro dimater pipes, D_{mm}>3)

APPENDIX B : Thermophysical Properties of Commonly Known Refrigerants

APPENDIX C : Compiled experimental datas collected from different sources

APPENDIX A Correlations for conventional pipes (macro dimater pipes, mm>3)

Table A.1 Correlations for conventional pipes (macro dimater pipes, mm>3)

Kandlikar

$\alpha_k = \max(E,S)\cdot\alpha_{lo}$ Co=((1-x)/x)$^{0.8}\cdot(\rho_v/\rho_l)^{0.5}$

$F_{Fl}=1$

$Fr_l \geq 0.04$ $F_{Ff}=1$

$Fr_l < 0.04$ $Fr_f=(25\cdot Fr_l)^{0.3}$

$S=(1.136\cdot Co^{-0.9}\cdot Fr_f)+(667.2\cdot Bo^{0.7}\cdot F_{Fl})$

$E=(0.6683\cdot Co^{-0.2}\cdot Fr_f)+(667.2\cdot Bo^{0.7}\cdot F_{Fl})$

Steiner and Taborek

$$\alpha_{st}=\left[(E\cdot\alpha_{lo})^3+(S\cdot\alpha_{tp})^3\right]^{1/3}$$

$$S=F\cdot\left(\frac{q}{1.5\cdot10^5}\right)^{0.8-0.1\exp(1.75P_{red})}\left(\frac{D_h}{0.01}\right)^{-0.4}f(M_w)$$

$$F=2.816\cdot P_{red}^{\ 0.45}+\left(3.4+\frac{1.7}{1-P_{red}^{\ 7}}\right)\cdot P_{red}^{\ 3.7}$$

$$f(M_w)=0.377+0.199\cdot\log_{10}(M_w)+0.000028427\cdot M_w^{\ 2}$$

$$E=\left[(1-x)^{1.5}+1.9\cdot x^{0.6}\cdot\left(\frac{\rho_l}{\rho_v}\right)^{0.35}\right]^{1.1}$$

$$\alpha_{tp}=18890$$

Liu and Winterton

$$\alpha_{LW}=\left[(E\cdot\alpha_{lo})^2+(S\cdot\alpha_{tp})^2\right]^{1/2}$$

$Fr_l \leq 0.05$

$S=(1+1.15\cdot10^{-6}\cdot E^2\cdot \mathrm{Re}_l^{\ 1.17})^{-1}$

$E=1+24000\cdot \mathrm{Bo}^{1.16}+1.37\cdot(1/X_{tt})^{0.86}$

$$\alpha_{tp}=55P_{red}^{\ 0.12}(-\log_{10}(P_{red}))^{-0.55}M_w^{\ -0.5}q^{0.67}$$

$E' = E\cdot Fr_l^{\ 0.1-0.2Fr_l}$

$S' = S\cdot Fr_l^{\ 0.5}$

Table A.1 (continued) Correlations for conventional pipes (macro dimater pipes, mm>3)

Gungor & Winterton

$$\alpha_{GW} = (E \cdot \alpha_l) + (S \cdot \alpha_{tp})$$

$\mathrm{Fr}_l \le 0.05$ $\quad S=(1+1.15 \cdot 10^{-6} E^2 \mathrm{Re}_l^{1.17})^{-1}$

$$E=1+24000 \cdot \mathrm{Bo}^{1.16} + 1.37 \cdot (1/X_{tt})^{0.86}$$

$$\alpha_{tp} = 55 P_{red}^{0.12} (-\log_{10}(P_{red}))^{-0.55} M_W^{-0.5} q^{0.67}$$

$$E' = E \cdot Fr_l^{0.1-2Fr_l}$$

$$S' = S \cdot Fr_l^{0.5}$$

Cooper

$$\alpha_{CO} = \alpha_{tp}$$

$$\alpha_{tp} = 55 P_{red}^{0.12} (-\log_{10}(P_{red}))^{-0.55} M_W^{-0.5} q^{0.67}$$

Wattelet et al.

$$\alpha_{wat} = (\alpha_{tp,nb} + \alpha_{tp,cb})^{0.4}$$

$Fr_l \ge 0.25$ $\quad E = 1+1.925 X_{tt,Watt}^{-0.83}$

$Fr_l < 0.25$ $\quad \Omega = 0.551 P_{red}^{0.492}$

$$X_{tt,Watt} = \left(\frac{1-x}{x}\right)^{0.9} \Omega$$

$R=1$

$R=1.32\mathrm{Fr}_l^{0.2}$

$$\alpha_{tp,nb} = 55 P_{red}^{0.12} (-\log_{10}(P_{red}))^{-0.55} M_w^{-0.5} q^{0.67}$$

$$\alpha_{tp,cb} = E \cdot \alpha_l \cdot R$$

APPENDIX B : Thermophysical Properties of Commonly Known Refrigerants

Table B.1 : Thermophysical Properties of Commonly Known Refrigerants

Refrigerants	$T_{critical}$ (°C)	$P_{critical}$, (bar)	Liquid Phase Density (kg/m^3)	Vapour Phase Density (kg/m^3)	Thermal Capacity (kJ/kg)	Volumetric Capacity (kJ/m^3)	Heat conduction Coefficient (W/m.K)	Dynamic Viscosity (mPa.s)
R 11	198	44.1	1536.9	2.36	0.85	450.76	0.09	0.5
R 12	112	42.2	1400.1	17.185	0.93	2636.52	0.62	0.25
R 22	96.2	49.9	1285.7	20.41	1.16	4205.28	0.09	0.22
R 134a	101.1	40.6	1298.9	13.9	1.3	2773.75	0.09	0.27
R 410a	72.13	49.3	1175	28.82	1.5	6566.35	0.1	0.16
R 404a	72	37.3	1154.8	29.91	1.3	4953.99	0.07	0.18
R 407c	86.74	46.2	1240.8	18.86	1.4	3973.24	0.01	0.21
R 507a	70.6	37.05	1161.1	30.98	1.37	5055.32	0.072	0.18
R744 (CO2)	31	73.7	934.26	94.148	2.5	22089.00	0.11	0.101
R717 (NH3)	132.3	113.3	640.28	3.31	4.41	4192.51	0.56	0.172

APPENDIX C : Compiled experimental datas collected from different sources

Table C.1. Compiled experimental datas collected from different sources and darkened.

Dmm	x (vapor quality)	G[kg/m2s]	Q[kW/m2]	T_s[K]	p_{total}/p_{cr}-p_r reduced pressure	P_{tot} total pressure	M (kg/kmol)	viscosity (kg/ms) liquid	viscosity (kg/ms) vapor	c_{pL}(KJ/kgK) spesicif heat liquid	c_{pv}(KJ/kgK) spesicif heat vapor	Thermal (kW/mK) conduct.liquid	Thermal (kW/mK) cond.vapor	density liquid kg/m^3	density vapor kg/m^3	surface tension(kg/m)	Bo Bond Number	We_{liquid} Weber Number	We_{vapor} Weber Number	X_{tt} Martinelli Number	Re_V Reynold Vapor	Fr_l Froude Number liquid	Pr_l Liquid prandtl number	Prv Vapor prandtl number	ε Void fraction	Alan(m^2) AL(liquid phase section)	HTC[KW/m2K (experimental heat transfer coefficient)
0.0077	0.1080	424.0000	20.0000	273.0000	0.4724	3.4864	44.0100	99.4000	14.7900	2.5420	1.8650	0.0001	0.0000	927.4000	97.6563	0.0004	1,099.5240	3,381.5278	32,112.9355	2.6120	0.0519	2.7516	2,290,173.1170	1,444,948.7938	0.4605	0.0000	12.1420
0.0077	0.1930	424.0000	20.0000	273.0000	0.4724	3.4865	44.0100	99.4000	14.7900	2.5420	1.8650	0.0001	0.0000	927.4000	97.6563	0.0004	1,099.5240	3,381.5278	32,112.9355	1.4398	0.0697	2.7516	2,290,173.1170	1,444,948.7938	0.6130	0.0000	11.5940
0.0077	0.2880	424.0000	20.0000	273.0000	0.4724	3.4865	44.0100	99.4000	14.7900	2.5420	1.8650	0.0001	0.0000	927.4000	97.6563	0.0004	1,099.5240	3,381.5278	32,112.9355	0.9091	0.0891	2.7516	2,290,173.1170	1,444,948.7938	0.7151	0.0000	10.5280
0.0077	0.3800	424.0000	20.0000	273.0000	0.4724	3.4865	44.0100	99.4000	14.7900	2.5420	1.8650	0.0001	0.0000	927.4000	97.6563	0.0004	1,099.5240	3,381.5278	32,112.9355	0.6319	0.1076	2.7516	2,290,173.1170	1,444,948.7938	0.7818	0.0000	9.4620
0.0077	0.4740	424.0000	20.0000	273.0000	0.4724	3.4865	44.0100	99.4000	14.7900	2.5420	1.8650	0.0001	0.0000	927.4000	97.6563	0.0004	1,099.5240	3,381.5278	32,112.9355	0.4510	0.1260	2.7516	2,290,173.1170	1,444,948.7938	0.8326	0.0000	8.6090
0.0077	0.5650	424.0000	20.0000	273.0000	0.4724	3.4865	44.0100	99.4000	14.7900	2.5420	1.8650	0.0001	0.0000	927.4000	97.6563	0.0004	1,099.5240	3,381.5278	32,112.9355	0.3276	0.1434	2.7516	2,290,173.1170	1,444,948.7938	0.8719	0.0000	6.3710
0.0077	0.6540	424.0000	20.0000	273.0000	0.4724	3.4865	44.0100	99.4000	14.7900	2.5420	1.8650	0.0001	0.0000	927.4000	97.6563	0.0004	1,099.5240	3,381.5278	32,112.9355	0.2359	0.1601	2.7516	2,290,173.1170	1,444,948.7938	0.9041	0.0000	5.8380
0.0077	0.7490	424.0000	20.0000	273.0000	0.4724	3.4865	44.0100	99.4000	14.7900	2.5420	1.8650	0.0001	0.0000	927.4000	97.6563	0.0004	1,099.5240	3,381.5278	32,112.9355	0.1582	0.1775	2.7516	2,290,173.1170	1,444,948.7938	0.9341	0.0000	5.1980
0.0077	0.8410	424.0000	20.0000	273.0000	0.4724	3.4865	44.0100	99.4000	14.7900	2.5420	1.8650	0.0001	0.0000	927.4000	97.6563	0.0004	1,099.5240	3,381.5278	32,112.9355	0.0959	0.1939	2.7516	2,290,173.1170	1,444,948.7938	0.9600	0.0000	4.9850
0.0077	0.9350	424.0000	20.0000	273.0000	0.4724	3.4865	44.0100	99.4000	14.7900	2.5420	1.8650	0.0001	0.0000	927.4000	97.6563	0.0004	1,099.5240	3,381.5278	32,112.9355	0.0399	0.2102	2.7516	2,290,173.1170	1,444,948.7938	0.9842	0.0000	4.2230
.																											
.																											
.																											
.																											
.																											
.																											
0.0035	0.3950	402.0000	10.0400	243.0000	0.1935	1.4284	44.0100	164.2000	12.4600	2.0721	1.1389	0.0001	0.0000	1,075.7000	37.0920	0.0010	121.7988	511.5513	14,835.4346	0.3722	0.0508	4.0551	2,307,016.6802	1,067,491.1799	0.8784	0.0000	6.7860
0.0035	0.5537	400.2000	9.9280	243.0000	0.1935	1.4284	44.0100	164.2000	12.4600	2.0721	1.1389	0.0001	0.0000	1,075.7000	37.0920	0.0010	121.7988	506.9805	14,702.8774	0.2122	0.0677	4.0189	2,307,016.6802	1,067,491.1799	0.9194	0.0000	7.9500
0.0035	0.6949	400.6000	9.9750	243.0000	0.1935	1.4284	44.0100	164.2000	12.4600	2.0721	1.1389	0.0001	0.0000	1,075.7000	37.0920	0.0010	121.7988	507.9945	14,732.2831	0.1247	0.0825	4.0270	2,307,016.6802	1,067,491.1799	0.9479	0.0000	8.4480
0.0035	0.8241	396.7000	10.0100	243.0000	0.1935	1.4284	44.0100	164.2000	12.4600	2.0721	1.1389	0.0001	0.0000	1,075.7000	37.0920	0.0010	121.7988	498.1516	14,446.8302	0.0664	0.0946	3.9489	2,307,016.6802	1,067,491.1799	0.9710	0.0000	9.3860
0.0035	0.0875	407.1000	14.9800	243.0000	0.1935	1.4284	44.0100	164.2000	12.4600	2.0721	1.1389	0.0001	0.0000	1,075.7000	37.0920	0.0010	121.7988	524.6133	15,214.2438	1.9946	0.0157	4.1587	2,307,016.6802	1,067,491.1799	0.6369	0.0000	5.7120
0.0035	0.2486	401.3000	15.0200	243.0000	0.1935	1.4284	44.0100	164.2000	12.4600	2.0721	1.1389	0.0001	0.0000	1,075.7000	37.0920	0.0010	121.7988	509.7714	14,783.8139	0.6747	0.0342	4.0410	2,307,016.6802	1,067,491.1799	0.8184	0.0000	6.7100
0.0035	0.3994	398.8000	15.0900	243.0000	0.1935	1.4284	44.0100	164.2000	12.4600	2.0721	1.1389	0.0001	0.0000	1,075.7000	37.0920	0.0010	121.7988	503.4396	14,600.1886	0.3663	0.0509	3.9908	2,307,016.6802	1,067,491.1799	0.8797	0.0000	7.8040
0.0035	0.5509	401.5000	14.9700	243.0000	0.1935	1.4284	44.0100	164.2000	12.4600	2.0721	1.1389	0.0001	0.0000	1,075.7000	37.0920	0.0010	121.7988	510.2796	14,798.5535	0.2144	0.0676	4.0451	2,307,016.6802	1,067,491.1799	0.9188	0.0000	8.8230
0.0035	0.6933	402.5000	15.0400	243.0000	0.1935	1.4284	44.0100	164.2000	12.4600	2.0721	1.1389	0.0001	0.0000	1,075.7000	37.0920	0.0010	121.7988	512.8246	14,872.3616	0.1256	0.0827	4.0652	2,307,016.6802	1,067,491.1799	0.9476	0.0000	9.4910
0.0035	0.8178	401.9000	15.0600	243.0000	0.1935	1.4284	44.0100	164.2000	12.4600	2.0721	1.1389	0.0001	0.0000	1,075.7000	37.0920	0.0010	121.7988	511.2969	14,828.0547	0.0689	0.0952	4.0531	2,307,016.6802	1,067,491.1799	0.9699	0.0000	10.4630

CURRICULUM VITAE

Name Surname: Ahmet KORKMAZ

WORK EXPERIENCES

09.2021-Habaş Sınai Gazlar A.Ş - Current Job

09.2016-09.2021 Turkish Technic

6.2013-08.2016 SMS Group (Germany)

10.2010-03.2013 Ark Asansör